ATPase Mechanism of Eg5 in the Absence of Microtubules: Insight into Microtubule Activation and Allosteric Inhibition by Monastrol†

Jared C. Cochran and Susan P. Gilbert*

Department of Biological Sciences, University of Pittsburgh, Pittsburgh, Pennsylvania 15260

Received August 26, 2005; Revised Manuscript Received October 24, 2005

ABSTRACT: The ATPase mechanism of kinesin superfamily members in the absence of microtubules remains largely uncharacterized. We have adopted a strategy to purify monomeric human Eg5 (HsKSP/Kinesin-5) in the nucleotide-free state (apoEg5) in order to perform a detailed transient state kinetic analysis. We have used steady-state and presteady-state kinetics to define the minimal ATPase mechanism for apoEg5 in the absence and presence of the Eg5-specific inhibitor, monastrol. ATP and ADP binding both occur via a two-step process with the isomerization of the collision complex limiting each forward reaction. ATP hydrolysis and phosphate product release are rapid steps in the mechanism, and the observed rate of these steps is limited by the relatively slow isomerization of the Eg5−ATP collision complex. A conformational change coupled to ADP release is the rate-limiting step in the pathway. We propose that the microtubule amplifies and accelerates the structural transitions needed to form the ATP hydrolysis competent state and for rapid ADP release, thus stimulating ATP turnover and increasing enzymatic efficiency. Monastrol appears to bind weakly to the Eg5−ATP collision complex, but after tight ATP binding, the affinity for monastrol increases, thus inhibiting the conformational change required for ADP product release. Taken together, we hypothesize that loop L5 of Eg5 undergoes an "open" to "closed" structural transition that correlates with the rearrangements of the switch-1 and switch-2 regions at the active site during the ATPase cycle.

Motor proteins from the myosin, kinesin, and dynein superfamilies are important molecular machines that utilize the energy of ATP turnover to generate force and perform various functions in eukaryotic cells. These enzymes coordinate movements of conserved structural elements located at the nucleotide binding site (P-loop, switch-1, switch-2) with structural elements that interact with the filament surface (actin- or microtubule-binding interface) (*1*−*8*). The ATPase activity and enzymatic efficiency of these molecular motors are activated in the presence of their filament partner, which is thought to be mediated through acceleration of the rate of product release (reviewed in ref *9*). However, the structural basis for this phenomenon is not well understood.

The ATPase mechanisms of several different monomeric kinesins have been extensively studied in the presence of microtubules: conventional kinesin/Kinesin-1 (*10*−*12*), Eg5/Kinesin-5 (*13*), and Ncd/Kar3/Kinesin-14 (*14*−*16*). On the other hand, very little is known about the ATPase mechanism of kinesins in the absence of microtubules (*17*). Historically, kinesins have been purified with ADP bound to the nucleotide binding site (*18*), and attempts to isolate a homogeneous, nucleotide-free population have been difficult due to the instability of the catalytic domain in the absence of nucleotide (*14*, *17*).

The present studies were undertaken to define the minimal ATPase mechanism for monomeric human Eg5-367[1] (KSP/Kinesin-5) in the absence of microtubules. We adopted a purification strategy that yielded pure, stable, and fully active protein in the nucleotide-free state. We have employed a combination of steady-state and presteady-state kinetic methodologies to characterize the steps of ATP binding, ATP hydrolysis, P_i and ADP product release, and ADP product binding. We also performed experiments in the presence of the specific Eg5 inhibitor, monastrol, to elucidate the mechanistic basis of Eg5 inhibition in the absence of microtubules. A six-step pathway is suggested that is similar to the mechanism of Kinesin-1 ATPase (*17*). However, the rate of the isomerization to form the ATP hydrolysis competent intermediate was much slower and was nonproductive for a subpopulation of apoEg5 such that only a fraction of the Eg5 sites contributed to the formation of product during the first and subsequent ATP turnovers.

We propose that monastrol weakly binds the Eg5·ATP collision complex and alters the environment of the Eg5 nucleotide binding site. However, we cannot experimentally

† This work was supported by Grant GM54141 from NIGMS, National Institutes of Health (NIH), and through Career Development Award K02-AR47841 from NIAMS, NIH, Department of Health and Human Services (to S.P.G.).

* Corresponding author. Mailing address: A518 Langley Hall, 4249 Fifth Ave., Pittsburgh, PA 15260. Tel: 412-624-5842. Fax: 412-624-4759. E-mail: spg1@pitt.edu.

[1] Abbreviations: Eg5-367, human Eg5/KSP motor domain containing N-terminal 367 residues followed by a C-terminal His_6 tag; apoEg5, nucleotide-free Eg5-367; MDCC-PBP, 7-diethylamino-3-((((2-maleimidyl)ethyl)amino)carbonyl) coumarin-labeled phosphate binding protein; PNPase, purine nucleotide phosphorylase; MEG, 7-methylguanosine; P_i, inorganic phosphate; Mt, microtubule; HPLC, high performance liquid chromatography; AXP, any adenosine nucleotide; mant, 2′-(3′)-*O*-(*N*-methylanthraniloyl); AMPPNP, adenosine 5′-(β,γ-imino)triphosphate; FRET, fluorescence resonance energy transfer; BSA, bovine serum albumin; IgG, bovine gamma globulin; Oval, ovalbumin.

10.1021/bi051724w CCC: $30.25
Published on Web 11/23/2005

Table 1: Comparison of Kinetic Constants for ApoEg5 and Mt·Eg5 ATPase ± *S*-Monastrol

constants		apoEg5	apoEg5$_S$	Mt·Eg5[a,b]	Mt·Eg5$_S$[b]
MgATP binding	$K_1k_{+1'}$	0.037 ± 0.002 μM^{-1} s^{-1}	ND[c]	ND	ND
(Trp fluorescence)	$k_{+1'}$	0.54 ± 0.03 s^{-1}			
	$K_{d,}$ATP	2.6 ± 0.5 μM			
	$k_{-1'}$	0.014 ± 0.04 s^{-1}			
mantATP binding	$K_1k_{+1'}$	0.08 ± 0.01 μM^{-1} s^{-1}	0.06 ± 0.01 μM^{-1} s^{-1}	2.2 ± 0.3 μM^{-1} s^{-1}	2.1 ± 0.3 μM^{-1} s^{-1}
	$k_{+1'}$	0.85 ± 0.10 s^{-1}	0.78 ± 0.33 s^{-1}	47.0 ± 2.3 s^{-1}	47.8 ± 1.9 s^{-1}
	$K_{d,}$mATP	9.9 ± 2.6 μM	11.4 ± 7.9 μM	7.9 ± 1.6 μM	9.4 ± 1.9 μM
	$k_{-1'}$	0.09 ± 0.02 s^{-1}	0.09 ± 0.02 s^{-1}	18 ± 0.7 s^{-1}	19.1 ± 0.7 s^{-1}
	$K_{d,}$S		25.3 ± 13.5 μM		
ATP binding	$k_{b,}$max	1.7 ± 0.3 s^{-1}	1.3 ± 0.4 s^{-1}	20.8 ± 1.1 s^{-1} [d]	ND
(pulse-chase)	$K_{d,}$ATP	8.3 ± 6.3 μM	6.1 ± 7.6 μM	45 ± 8 μM	
	$A_{0,}$max	0.14 ± 0.01 ADP/site	0.14 ± 0.01 ADP/site	0.82 ± 0.1 ADP/site	
ATP hydrolysis	$k_{b,}$max	1.14 ± 0.05 s^{-1}	0.59 ± 0.04 s^{-1}	13.3 ± 1.5 s^{-1} [e]	48 ± 14 s^{-1} [e]
(acid-quench)	$K_{d,}$ATP	12.7 ± 2.0 μM	6.8 ± 2.1 μM		
	$A_{0,}$max	0.093 ± 0.002 ADP/site	0.15 ± 0.005 ADP/site	0.8 ± 0.04 ADP/site	0.3 ± 0.03 ADP/site
	$k_{ss,max}$/[Eg5]	0.017 ± 0.001 s^{-1}	0.008 ± 0.001 s^{-1}		
ATP hydrolysis	$k_{+1'}$[e]	1.03 ± 0.05 s^{-1}	0.57 ± 0.04 s^{-1}	11 ± 1 s^{-1} [f]	47 ± 13 s^{-1} [f]
(modeling)	k_{slow}	0.14 ± 0.003 s^{-1}	0.025 ± 0.002 s^{-1}	2.3 ± 0.2 s^{-1}	1.2 ± 0.3 s^{-1}
	E_0	0.5 of 4 μM (13%)	0.7 of 4 μM (18%)	4.7 of 5 μM (95%)	1.5 of 5 μM (30%)
P_i release	$k_{b,}$max	0.54 ± 0.01 s^{-1}	0.45 ± 0.01 s^{-1}	5.7 ± 0.02 s^{-1} [g]	ND
(MDCC-PBP)	$K_{d,}$ATP	6.3 ± 0.3 μM	5.1 ± 0.4 μM		
	$A_{0,}$max	0.10 ± 0.003 P_i/site	0.14 ± 0.002 P_i/site	0.70 ± 0.001 P_i/site	
	$k_{ss,max}$/[Eg5]	0.019 ± 0.0001 s^{-1}	0.003 ± 0.0001 s^{-1}		
P_i release	$k_{+1'}$	0.42 ± 0.006 s^{-1}	0.44 ± 0.003 s^{-1}	4.9 ± 0.02 s^{-1} [g]	
(modeling)	k_{slow}	0.14 ± 0.001 s^{-1}	0.022 ± 0.0005 s^{-1}	0.8 ± 0.001 s^{-1}	
	E_0	0.19 of 1 μM (19%)	0.15 of 1 μM (15%)	0.99 of 1 μM (99%)	
[α-^{32}P]ADP Release[b]	$k_{off,}$ADP	0.05 ± 0.001 s^{-1}	0.007 ± 0.001 s^{-1}		
mantADP release		ND	ND	35.2 ± 0.6 s^{-1}	13 ± 1 s^{-1}
mantADP binding	$K_{-5}k_{-4}$	0.07 ± 0.01 μM^{-1} s^{-1}	0.08 ± 0.02 μM^{-1} s^{-1}	ND	ND
	k_{-4}	0.55 ± 0.04 s^{-1}	1.3 ± 0.4 s^{-1}		
	$K_{1/2,}$mADP	6.5 ± 1.4 μM	13.1 ± 7.7 μM		
	k_{+4}	0.13 ± 0.01 s^{-1}	0.08 ± 0.03 s^{-1}		
	$K_{d,}$S		23.4 ± 4.8 μM		
basal ATPase	k_{cat}	0.02 ± 0.003 s^{-1}	0.003 ± 0.0001 s^{-1} [h]		
	$K_{m,}$ATP	0.17 ± 0.03 μM	0.19 ± 0.05 μM[h]		
	$k_{cat}/K_{m,}$ATP	0.12 ± 0.01 μM^{-1} s^{-1}	0.016 ± 1.4 μM^{-1} s^{-1} [h]		
	$K_{d,}$S		2.3 ± 0.4 μM[b]		
Mt-activated ATPase	k_{cat}	5.47 ± 0.07 s^{-1}	ND	5.5 ± 0.3 s^{-1}	1.2 ± 0.03 s^{-1}
	$K_{m,}$ATP	6.95 ± 0.43 μM		9.5 ± 0.4 μM	3.6 ± 0.3 μM
	$k_{cat}/K_{m,}$ATP	0.79 ± 0.16 μM^{-1} s^{-1}		0.58 ± 0.03 μM^{-1} s^{-1}	0.33 ± 0.03 μM^{-1} s^{-1}
	$K_{1/2,}$Mt	0.29 ± 0.02 μM		0.71 ± 0.6 μM	6.7 ± 0.4 μM
	$K_{d,}$S				13.8 ± 1.0 μM

[a] Mechanistic analysis of the mitotic kinesin Eg5 (*13*). [b] Monastrol inhibition of the mitotic kinesin Eg5 (*22*). [c] ND, not determined. [d] Experiments performed with monomeric HsEg5-437 (*13*). [e] $k_{+1'}$ = the rate of the isomerization of the Eg5·ATP collision complex. [f] Burst kinetics based on 300 μM MgATP (*22*). [g] Fit of data from transient shown in Figure 10D. [h] Determined from the linear phase of the P_i product release transients.

detect monastrol binding to apoEg5 in the absence of microtubules and/or nucleotide. The isomerization of the Eg5·ATP collision complex that occurs during the Eg5 ATPase mechanism leads to an "open" to "closed" structural transition in loop L5 to tighten Eg5's affinity for both ATP and monastrol. We propose that monastrol stabilizes the "closed" conformation of loop L5 and, after rapid ATP hydrolysis and P_i product release, inhibits the very slow isomerization of the Eg5*·ADP complex, which corresponds to the observed rate of ADP release. Therefore, these studies have enabled us to hypothesize a structural communication pathway between the functional elements at the Eg5 nucleotide binding site and loop L5. By comparing the Eg5 ATPase mechanism in the absence of microtubules to the microtubule-activated mechanism (*13*), we can also gain insight into how the microtubule activates the Eg5 ATPase cycle.

MATERIALS AND METHODS

Experimental Conditions. All experiments reported were performed at 22−25 °C in ATPase buffer (20 mM Hepes, pH 7.2 with KOH, 5 mM magnesium acetate, 0.1 mM EDTA, 0.1 mM EGTA, 50 mM potassium acetate, 1 mM dithiothreitol, 5% sucrose) with the concentrations reported as final after mixing. Experiments containing monastrol were performed using the more active *S*-enantiomer (*19*−*22*).

Purification of ApoEg5. In this study we have expressed and purified Eg5-367 as described previously (*13*, *19*), with the following modifications in order to isolate Eg5 in the absence of nucleotide at the active site (apoEg5) (*17*, *23*). In all column chromatography buffers, magnesium chloride and ATP were excluded. After Eg5 was eluted from the nickel−nitrilotriacetic acid agarose column (Qiagen, Valencia, CA), the enriched fractions were pooled and incubated with 5 mM EGTA and 5 mM EDTA for 30 min at 4 °C. Following the incubation, the mixture was loaded onto a 100-mL Bio-Gel P-6 size exclusion column (Bio-Rad Laboratories Inc.; exclusion limit 6000 Da) to remove chelating reagents and any residual nucleotide. The elution volume containing the excluded apoEg5 was concentrated by ultrafiltration and dialyzed against ATPase buffer. We determined the apoEg5 protein concentration by the Bio-Rad protein assay with IgG as the standard. This purification strategy yielded >99% pure protein with >95% basal and microtubule-activated ATPase activity under the same experimental conditions when compared to prior Eg5 purifications [Table 1 (*13*)]. In addition, we performed pulse-chase, acid-quench,

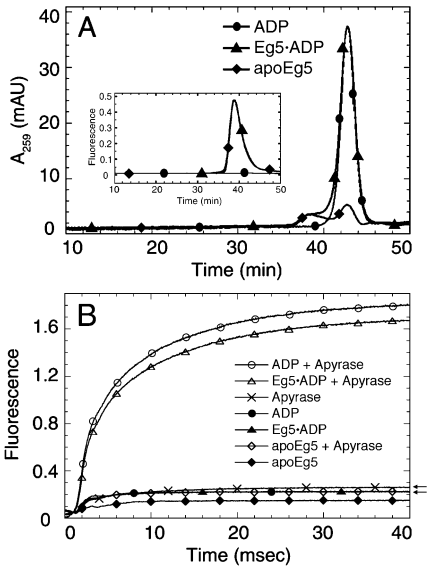

FIGURE 1: Determination of the nucleotide-free state for apoEg5. (A) Analytical gel filtration was performed using a Superose-6 HR column with detection by continuous monitoring of solution absorbance at 259 nm (λ_{max} for ADP) and intrinsic protein fluorescence (inset). Conditions: 10 μM apoEg5, 10 μM Eg5·ADP, 10 μM MgADP. Eg5 eluted from the column at 38.8 min, MgADP eluted at 42.7 min, and the void volume eluted at 16.2 min. (B) Inorganic phosphate liberated from apyrase cleavage of ADP to AMP + P_i was detected by monitoring the fluorescence enhancement of MDCC-PBP·P_i in a stopped-flow instrument. Final concentrations: 1 μM apoEg5, 1 μM Eg5·ADP (1 μM apoEg5 + 1 μM MgADP), 1 μM MgADP, 0.05 unit/mL apyrase, 5 μM MDCC-PBP, 0.05 unit/mL PNPase, 75 μM MEG. ApoEg5 only, MgADP only, and Eg5·ADP (1:1) were incubated in the absence or presence of apyrase for 60 min at room temperature, followed by rapid mixing with MDCC-PBP plus "P_i mop" reagents. Transients for MgADP only, Eg5·ADP, and apoEg5 + apyrase overlay each other. Arrows highlight difference between transients for apoEg5 + apyrase and apyrase only.

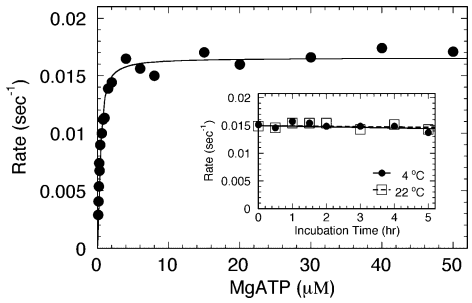

FIGURE 2: ApoEg5 steady-state ATPase. ApoEg5 was reacted with increasing MgATP concentrations in the absence of microtubules. Final concentrations: 0.1 μM apoEg5, 0.25 mg/mL BSA, 0.1−50 μM [α-^{32}P]MgATP. The data were fit to eq 1: $k_{cat} = 0.017 \pm 0.0003$ s^{-1} and $K_{m,ATP} = 0.17 \pm 0.03$ μM. Inset: apoEg5 stability was determined by measuring ATPase activity at various time points after incubation. Final concentrations: 0.5 μM apoEg5, 10 μM [α-^{32}P]MgATP, 4 °C or 22 °C incubation temperature. The ATPase reactions were performed at 22 °C, and the rate of MgATP turnover was plotted as a function of incubation time. The fit of the data to a single-exponential decay provided a rate constant at 0.004 ± 0.003 h^{-1} at both incubation temperatures.

and P_i product release experiments with apoEg5 in the presence of microtubules, and observed a burst stoichiometry near unity (Figure 8B−D), suggesting that the entire population of apoEg5 enzyme binds and hydrolyzes ATP during the first ATP turnover.

Nucleotide-Free Determination of ApoEg5 Preparation. Purified apoEg5 protein was resolved by using a Superose-6 HR 10/30 gel filtration column (Amersham Biosciences) that was equilibrated in ATPase buffer using the System Gold HPLC system (Beckman Coulter Inc.) (Figure 1A). The elution profiles were obtained by continuous monitoring of solution absorbance at 259 nm (λ_{max} for ADP) and intrinsic protein fluorescence (Ex, 280 nm; Em, 340 nm) at a constant flow rate of 0.5 mL/min. The duration of the elution provides time for >100 ADP release events to occur at each Eg5 site ($k_{off,ADP} = 0.05-0.14$ s^{-1}), thus allowing any remaining ADP bound at the Eg5 nucleotide binding site to be released and diffuse into the included volume of the column. The elution profile of ADP in the absence of Eg5 was compared to the elution profiles of apoEg5 and Eg5·ADP (1:1) to quantify the nucleotide that remained in each apoEg5 preparation. ImageGauge (version 4.0) software (Fuji Photo Film USA) was used to analyze the data.

We designed another experiment to assess the nucleotide-free state of our apoEg5 preparation. By treating a sample of apoEg5 with apyrase (Sigma-Aldrich Co.; type VII) for 60 min, any remaining ADP bound to Eg5 would be released into solution and cleaved to AMP + P_i. Using a coupled-assay system with coumarin-labeled phosphate binding protein (MDCC-PBP), as described (*24*, *25*), we were able to directly measure P_i liberated from the apyrase cleavage reaction. Any P_i in solution would bind to the MDCC-PBP and induce a fluorescence enhancement. Apyrase-treated samples of apoEg5, Eg5·ADP (1:1), and ADP (no Eg5) were rapidly mixed in a KinTek SF-2003 stopped-flow instrument (KinTek Corp., Austin, TX) with MDCC-PBP (Ex, 425 nm; Em, 450-nm cutoff) (Figure 1B). Contaminating P_i was removed from the MDCC-PBP solution, stopped-flow syringes, and observation cell by incubation with a "P_i mop" consisting of 0.05 unit/mL purine nucleotide phosphorylase (PNPase) and 75 μM 7-methylguanosine (MEG). However, the Eg5 and ADP samples were not incubated with the "P_i mop" prior to mixing with the MDCC-PBP.

Steady-State ATPase Kinetics. ApoEg5 steady-state ATPase activity (in the absence of microtubules) was determined by measuring [α-^{32}P]ADP·P_i product formation as described previously (*26*). In Figure 2, the rate of ATP turnover was plotted as a function of MgATP concentration, and the data were fit to the following quadratic equation:

$$\text{rate} = 0.5k_{cat}\{(E_0 + K_{m,ATP} + [ATP]) - \{(E_0 + K_{m,ATP} + [ATP])^2 - (4E_0[ATP])\}^{1/2}\} \quad (1)$$

where rate is the concentration of product formed per second per Eg5 site, k_{cat} is the maximum rate constant of product formation at saturating substrate, E_0 is the total Eg5 site concentration, and $K_{m,ATP}$ is the MgATP concentration needed to provide one-half the maximal velocity.

ApoEg5 stability was determined by monitoring the ATPase activity (no microtubules) at various time points after incubation at either 4 °C or 22 °C (Figure 2, inset). The observed steady-state rates as a function of incubation time were fit to a single-exponential decay. In Figure 8A, apoEg5 steady-state ATPase was determined in the absence and presence of 0.25 mg/mL bovine serum albumin (BSA, BioRad), bovine gamma globulin (IgG, BioRad), or oval-

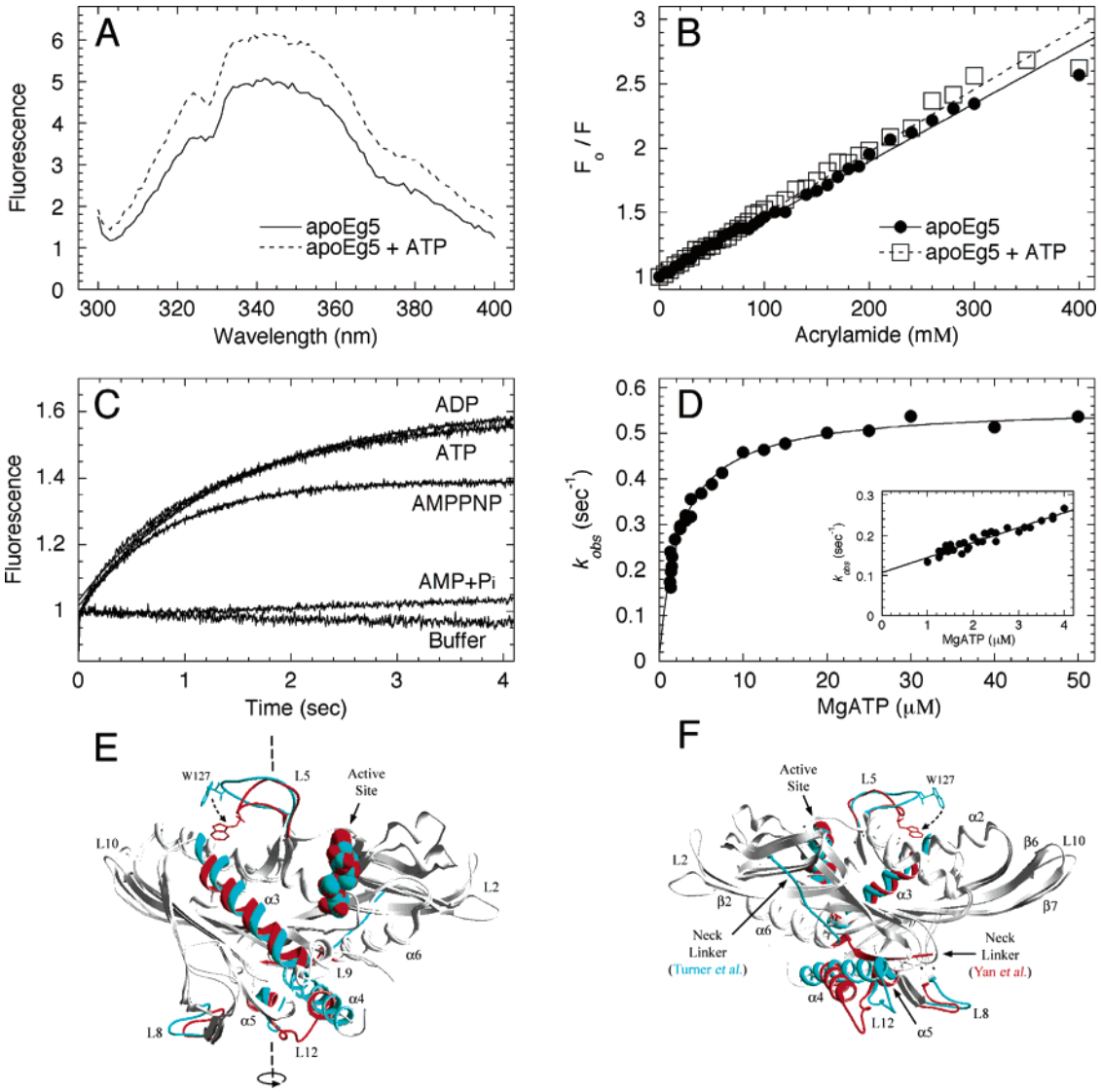

FIGURE 3: MgATP binding to apoEg5 by tryptophan fluorescence enhancement. (A) The steady-state fluorescence emission spectra of apoEg5 in the absence and presence of MgATP. Final concentrations: 2 μM apoEg5, 0 or 200 μM MgATP. (B) Stern−Volmer plot for acrylamide quenching of apoEg5 tryptophan fluorescence in the absence or presence of MgATP. Final concentrations: 2 μM apoEg5, 0 or 500 μM MgATP, 0−400 mM acrylamide. Relative fluorescence intensity changes from quenching (F_o/F) were plotted against acrylamide concentration, and each data set was fit to eq 2. ApoEg5: $K_{sv} = 4.5 \pm 0.5$ M^{-1}. apoEg5 + ATP: $K_{sv} = 4.9 \pm 0.6$ M^{-1}. (C) The transient increase in apoEg5 tryptophan fluorescence upon rapid mixing with various nucleotides in a stopped-flow instrument. Final concentrations: 2 μM apoEg5, 250 μM MgAXP (as indicated). MgAMP + P_i conditions were achieved by incubating 250 μM MgADP with 0.1 unit/mL apyrase for 60 min, followed by mixing in a stopped-flow instrument. (D) The observed exponential rate of MgATP binding to apoEg5 was plotted as a function of MgATP concentration. Final concentrations: 1 μM apoEg5, 1.25−100 μM MgATP. The data were fit to eq 3: $k_{+1'} = 0.54 \pm 0.03$ s^{-1}, $k_{-1'} = 0.014 \pm 0.03$ s^{-1}, and $K_{d,ATP} = 2.6 \pm 0.5$ μM. Note that the constant $k_{-1'}$ has a significant error due to the loss of sensitivity below 1 μM apoEg5. Inset: The rates of MgATP binding to apoEg5 at low MgATP concentrations. The data were fit to a linear relationship to yield the apparent second-order rate constant defined by the slope ($K_1k_{+1'} = 0.037 \pm 0.002$ μM^{-1} s^{-1}) and the apparent rate of Eg5·ATP dissociation defined by the *y*-intercept ($k_{-1}^{app} = 0.11 \pm 0.01$ s^{-1}). (E and F) Structural representation of the proposed conformational change in loop L5 leading to the enhanced tryptophan fluorescence upon tight ATP binding. The model was generated using DeepView Swiss Pdb Viewer (version 3.7) to superposition the Eg5·ADP structure [PDB code: 1II6 (*30*); labeled blue] with the monastrol·Eg5·ADP structure [PDB code: 1Q0B (*21*); labeled red] based on the position of C_α atoms of the P-loop region (F102−T112). The microtubule-binding region was oriented at the bottom and loop L5 was visible at the top in both panels. Panel F depicts a view of the model after rotating ~180° around the axis indicated in panel E.

bumin (Oval, Sigma). These reactions were performed to evaluate the potential loss of apoEg5 active sites by adsorption of apoEg5 to the reaction tubes.

Fluorescence Measurements. Steady-state fluorescence measurements of the single Eg5 tryptophan (W127) and 2′(3′)-*O*-(*N*-methylanthraniloyl) (mant) nucleotides were obtained at 22 °C using an Aminco-Bowman Series 2 luminescence spectrometer (Thermo Spectronic, Madison, WI) equipped with a 150-W continuous wave xenon arc lamp source. ApoEg5 samples were excited at 295 nm (2-nm half-width), and tryptophan emission spectra were scanned from 300 to 400 nm (2-nm half-width) (Figure 3A). The appropriate buffer controls were subtracted from each spectrum to adjust for Raman scatter and background fluorescence. Mant-emission spectra were obtained by exciting the solution at 360 nm (4-nm half-width) and collecting emitted fluorescence from 400 to 600 nm (2-nm half-width) (Figure 4E). MantATP was used at 10 μM in

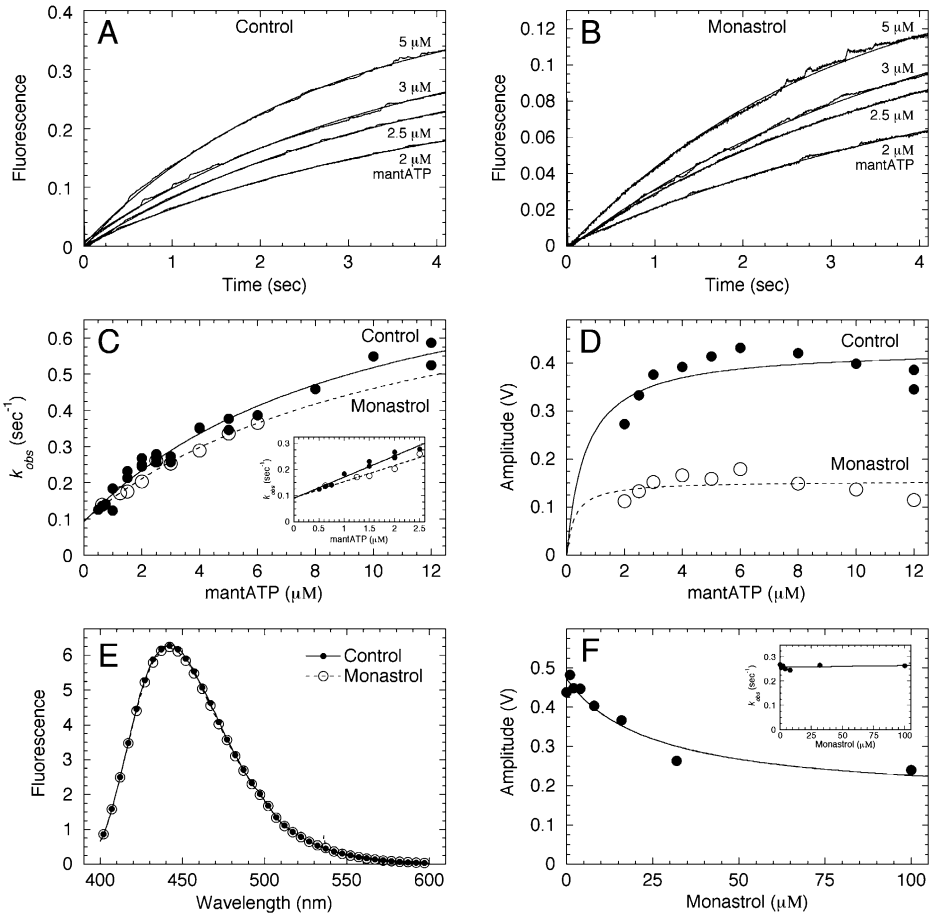

FIGURE 4: MantATP binding to apoEg5 ± monastrol. Representative stopped-flow transients are shown for mantATP binding to apoEg5 in the absence (A) and presence (B) of monastrol. Final concentrations: 0.5 μM apoEg5 for 0.5−2 μM mantATP, 2 μM apoEg5 for 2−12 μM mantATP, 0 or 150 μM monastrol. (C) The observed exponential rate of mantATP binding to apoEg5 was plotted as a function of mantATP concentration. Each data set was fit to eq 3. Control: $k_{+1'} = 0.85 \pm 0.1$ s^{-1}, $k_{-1'} = 0.09 \pm 0.02$ s^{-1}, and $K_{d,mATP} = 9.9 \pm 2.6$ μM. Monastrol: $k_{+1'} = 0.78 \pm 0.33$ s^{-1}, $k_{-1'} = 0.09 \pm 0.02$ s^{-1}, and $K_{d,mATP} = 11.4 \pm 7.9$ μM. Inset: The rates of mantATP binding to apoEg5 at low mantATP concentrations. The data were fit to a linear relationship to yield the apparent second-order rate constant defined by the slope ($K_1 k_{+1'} = 0.081 \pm 0.006$ μM^{-1} s^{-1} and 0.062 ± 0.01 μM^{-1} s^{-1} for control and monastrol, respectively) and the apparent rate of Eg5•mantATP dissociation defined by the *y*-intercept ($k_{-1}^{app} = 0.09 \pm 0.01$ s^{-1} for both). (D) The amplitude of each transient was plotted against mantATP concentration, and each data set was fit to a hyperbola. Maximum amplitude was 0.43 ± 0.03 V for control and 0.15 ± 0.02 V for monastrol. (E) The emission spectra of mantATP (no Eg5) in the absence and presence of monastrol. Final concentrations: 10 μM mantATP, 0 or 150 μM monastrol. (F) The amplitude of mantATP binding transients was plotted as a function of monastrol concentration, and the data were fit to eq 4. Final concentrations: 1 μM apoEg5, 2.5 μM mantATP, 0−100 μM monastrol. From the fit of the data, $K_{d,S}$ was 25.3 ± 13.5 μM. The inset shows the observed rate of mantATP binding plotted against monastrol concentration.

Scheme 1

$$\mathrm{E + ATP} \underset{}{\overset{K_1}{\rightleftharpoons}} \mathrm{E{\bullet}ATP} \underset{k_{-1'}}{\overset{k_{+1'}}{\rightleftharpoons}} \mathrm{E^{*}{\bullet}ATP} \overset{k_{+2}}{\rightleftharpoons} \mathrm{E{\bullet}ADP{\bullet}P_i} \overset{k_{+3}}{\rightleftharpoons} \mathrm{E{\bullet}ADP} \overset{k_{+4}}{\rightleftharpoons} \mathrm{E + ADP}$$

order to avoid inner-filter effects associated with the mant probe.

Acrylamide Quenching Experiment. To determine the relative solvent accessibility of the W127 residue, acrylamide quenching experiments were performed in the absence and presence of ATP. The fluorescence values from 340 nm in the absence of quencher (F_0) were divided by the fluorescence in the presence of quencher (F). These values were plotted as a function of quencher concentration ([Q]), and each data set was fit to the Stern−Volmer equation (Figure 3B):

$$F_0/F = 1 + K_{sv}[Q] \qquad (2)$$

where K_{sv} is the Stern−Volmer quenching constant, which equals the product of the bimolecular quenching constant (k_q) and the lifetime of the tryptophan fluorophore in the absence of quencher (τ_0).

Stopped-Flow Experiments. Presteady-state kinetic measurements of MgATP binding, mantATP binding, P_i product release, and mantADP binding were made in a stopped-flow instrument (KinTek Corp.). For tryptophan fluorescence experiments (Figure 3C,D), fluorescence emission at 340 nm was measured using a 340-nm specific band-pass filter with excitation at 295 nm. MgATP and mantATP binding data shown in Figure 3D and Figure 4C, respectively, were fit to the following equation:

$$k_{obs} = k_{+1'}[ATP]/(K_{d,ATP} + [ATP]) + k_{-1'} \qquad (3)$$

where $k_{+1'}$ equals the rate constant for the ATP-dependent isomerization (Scheme 1), $k_{-1'}$ is the ATP off rate, and

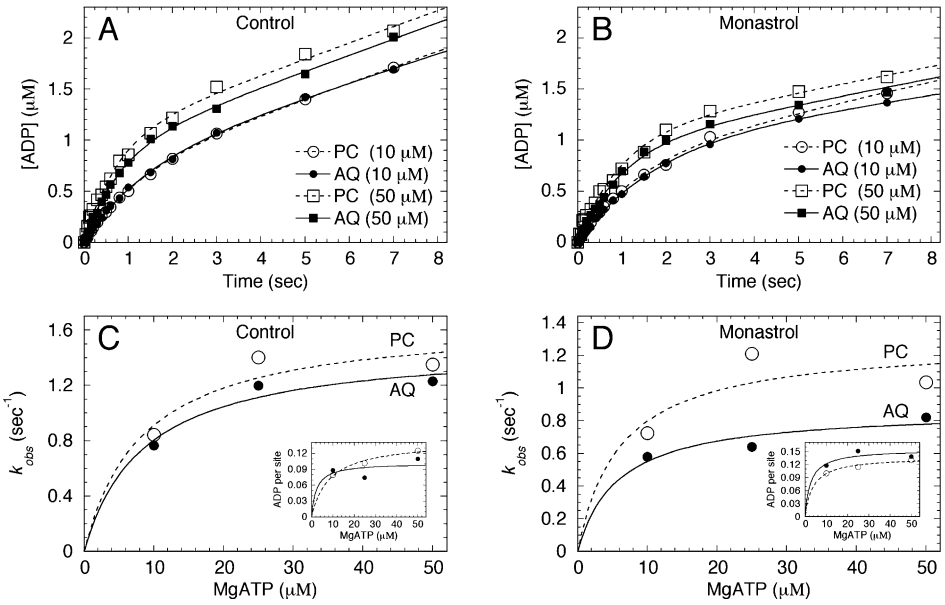

FIGURE 5: MgATP binding to apoEg5 by pulse-chase ± monastrol. ApoEg5 was reacted with [α-^{32}P]MgATP for 0−7 s in a chemical quench-flow instrument, followed by the nonradioactive MgATP chase for 8 min (>10 turnovers). Final concentrations: 8 μM apoEg5, 0 or 150 μM monastrol, 10−50 μM [α-^{32}P]MgATP, 10 mM unlabeled MgATP chase. Shown are time courses of [α-^{32}P]MgADP product formation for pulse-chase (PC) and acid-quench (AQ) experiments (similar to Figure 6; see below) in the absence (A) and presence (B) of monastrol (MgATP concentrations are indicated). Each transient displayed burst kinetics and was fit to eq 6 to provide the amplitude (A_0) and observed exponential rate (k_b) of the formation of a tight Eg5*•ATP complex (pulse-chase) or the formation of Eg5•ADP•P_i complex (acid-quench), followed by the linear steady-state ATP turnover (k_{ss}). Shown are the maximum observed rates from the pulse-chase and acid-quench experiments in the absence (C) and presence (D) of monastrol plotted against MgATP concentration. Each data set was fit to a hyperbola. Control: $k_{b,max} = 1.7 \pm 0.3$ s^{-1} for PC and 1.5 ± 0.2 s^{-1} for AQ. Monastrol: $k_{b,max} = 1.3 \pm 0.4$ s^{-1} for PC and 0.9 ± 0.1 s^{-1} for AQ. Insets show amplitude of exponential phase versus MgATP concentration, with each data set fit to a hyperbola. Control: pulse-chase $A_0 = 0.14 \pm 0.01$ ADP/site and acid-quench $A_0 = 0.10 \pm 0.03$ ADP/site. Monastrol: pulse-chase $A_0 = 0.14 \pm 0.01$ ADP/site and acid-quench $A_0 = 0.15 \pm 0.02$ ADP/site.

Scheme 2

$$E^*\cdot ADP \underset{k_{-4}}{\overset{k_{+4}}{\rightleftharpoons}} E\cdot ADP \overset{K_S}{\rightleftharpoons} E + ADP$$

$K_{d,ATP}$ is the dissociation constant for weak ATP binding. In Figure 4F and Figure 10D, the data were fit to the following quadratic equation:

$$\text{amplitude} = -0.5\{(A_{inh} + K_{d,S} + [Mon]) - \{(A_{inh} + K_{d,S} + [Mon])^2 - (4A_{inh}[Mon])\}^{1/2}\} + A_{max} \quad (4)$$

where amplitude is the magnitude of the exponential change in fluorescence intensity upon mantATP binding, A_{inh} is the amplitude of monastrol inhibition defined by A_{max} (amplitude at no monastrol) minus A_{min} (amplitude at saturating monastrol), $K_{d,S}$ is the apparent dissociation constant for monastrol, and Mon is the monastrol concentration. MantADP binding data shown in Figure 10B were fit to the following equation:

$$k_{obs} = k_{-4}[mADP]/(K_{1/2,mADP} + [mADP]) + k_{+4} \quad (5)$$

where k_{-4} equals the forward rate constant for the ADP-dependent isomerization (Scheme 2), k_{+4} equals the reverse rate constant correlated with the ADP off-rate, and $K_{1/2,mADP}$ is the mantADP concentration required to provide half the maximal rate.

The kinetics of P_i product release from apoEg5 were measured using the MDCC-PBP coupled-assay (*24*). ApoEg5 plus MDCC-PBP and "P_i mop" were rapidly mixed with increasing MgATP concentrations plus "P_i mop". The concentrations of the "P_i mop" reagents were experimentally determined to eliminate competition with the MDCC-PBP for P_i in solution (*27*). The experimental design assumes that, after ATP hydrolysis, P_i product will be released from the Eg5 active site, followed immediately by P_i binding rapidly and tightly to MDCC-PBP, thus triggering the fluorescence enhancement of the MDCC-PBP•P_i complex (*24*). This experimental design cannot detect reversibility at the P_i release step where P_i rebinds the Eg5 nucleotide binding site. To convert the observed change in fluorescence into units of P_i concentration, a phosphate calibration curve was used (Figure 7D, inset). The data in Figure 7A,B and Figure 8D show a burst of P_i product release at a rate faster than a subsequent rate-limiting step; thus the data were fit to the following equation to describe the time dependence of product release:

$$[product]_{obs} = A_0[1 - \exp(-k_b t)] + k_{ss} t \quad (6)$$

where A_0 equals the amplitude of the exponential burst phase, k_b is the observed exponential rate of P_i product release from apoEg5, and k_{ss} is the slope of the linear phase corresponding to subsequent ATP turnovers.

Quench-Flow Experiments. The presteady-state kinetics of MgATP binding and ATP hydrolysis (Figures 5, 6, 8) were determined by utilizing pulse-chase and acid-quench methodologies, respectively (*13*), using a KinTek RQF-3 chemical quench-flow instrument (KinTek Corp.). In the acid-quench experiments, apoEg5 was rapidly mixed with increasing concentrations of [α-^{32}P]MgATP, and the reaction continued for various times (0.04−7 s) followed by quench-

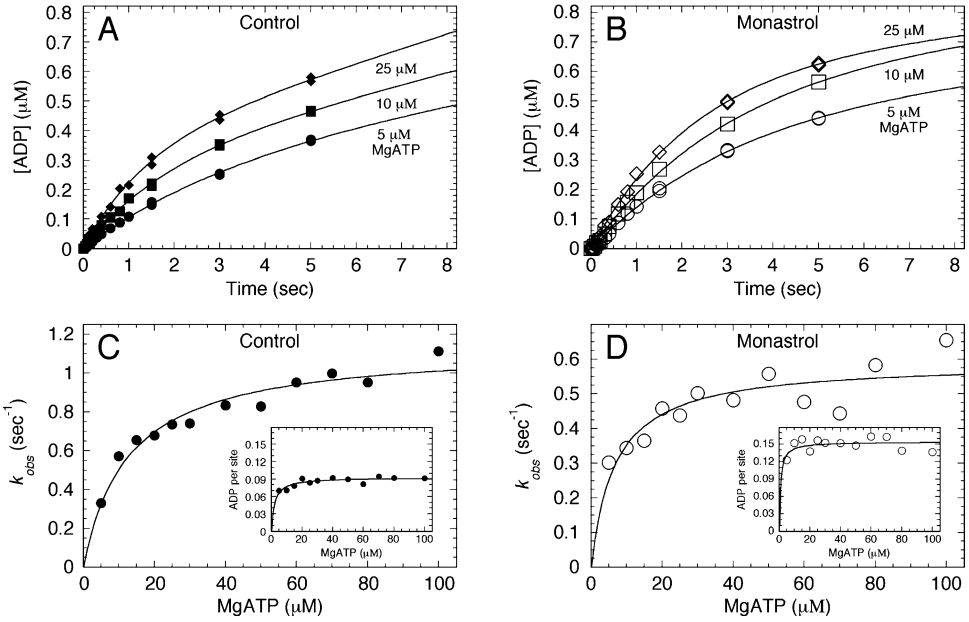

FIGURE 6: Presteady-state kinetics of ATP hydrolysis ± monastrol. Time course of [α-^{32}P]MgADP·P_i product formation after rapidly mixing apoEg5 in the absence (A) or presence (B) of monastrol with increasing MgATP concentrations in a chemical quench-flow instrument. Final concentrations: 4 μM apoEg5, 5−100 μM [α-^{32}P]MgATP, 0 or 150 μM monastrol. (C) The observed exponential rate of product formation in the absence of monastrol was plotted as a function of MgATP concentration. The data were fit to a hyperbola to define the maximum observed rate of ATP hydrolysis, $k_{b,max} = 1.14 \pm 0.05$ s^{-1} and $K_{d,ATP} = 12.7 \pm 2.0$ μM. Inset: The amplitude of the exponential burst phase was plotted versus MgATP, and the data were fit to a hyperbola: $A_{0,max} = 0.093 \pm 0.002$ ADP/site (13% of expected amplitude based on Eg5 site concentration). (D) The exponential burst rate in the presence of monastrol was plotted as a function of MgATP concentration: $k_{b,max} = 0.59 \pm 0.04$ s^{-1} and $K_{d,ATP} = 6.8 \pm 2.1$ μM. Inset: The burst amplitude was plotted versus MgATP: $A_{0,max} = 0.15 \pm 0.005$ ADP/site (18% of expected amplitude).

ing with formic acid. The concentration of [α-^{32}P]ADP was plotted as function of time, and each transient was fit to eq 6 (Figure 5A,B, Figure 6A,B, Figure 8B,C). For eq 6, A_0 corresponds to the concentration of [α-^{32}P]ADP·P_i formed at the active site during the first ATP turnover, and k_b is the rate constant of this exponential phase of product formation.

In the pulse-chase experiments, apoEg5 was rapidly mixed with increasing concentrations of [α-^{32}P]MgATP, and the reaction continued for various times (0.04−7 s) followed by the nonradioactive MgATP chase (10 mM) for 8 min (>10 turnovers). The concentration of [α-^{32}P]ADP was plotted as function of time, and each transient was fit to eq 6 (Figure 5A,B). For eq 6, A_0 corresponds to the fraction of tightly bound Eg5*·ATP that proceeds in the forward direction toward ATP hydrolysis, and k_b is the rate constant of the exponential phase. For both pulse-chase and acid-quench experiments, the amplitude and observed rate of the exponential burst phase for each transient were plotted against MgATP concentration, and each data set was fit to a hyperbola.

Modeling Acid-Quench and P_i Product Release Kinetics. In Figure 7E,F, the P_i release kinetics were modeled in terms of a two-step irreversible mechanism, where the amplitude and rate constants were defined by

$$A_0 = E_0\{[k_{+1'}/(k_{+1'} + k_{slow})]^2\} \quad (7)$$

$$k_b = k_{+1'} + k_{slow} \quad (8)$$

$$k_{ss} = E_0[k_{+1'}k_{slow}/(k_{+1'} + k_{slow})] \quad (9)$$

where E_0 is the apoEg5 site concentration that reports during the first ATP turnover, $k_{+1'}$ denotes the rate constant for the slow isomerization step prior to ATP hydrolysis and P_i product release that limits the observed rate of P_i product release (Scheme 1), and k_{slow} is the rate constant of the slow step that occurs after P_i product release for apoEg5 and limits steady-state ATP turnover. We allowed E_0, $k_{+1'}$, and k_{slow} to float in the analysis due to the unknown Eg5 site concentration that contributed to the first ATP turnover event.

We used DynaFit software (BioKin Ltd., Pullman, WA) to model the acid-quench and P_i product release kinetics at 10, 25, and 50 μM MgATP to the mechanism proposed in Scheme 1 (*28*). For our acid-quench transients, we modeled the formation of ADP product, which represents Eg5·ADP·P_i + Eg5·ADP + ADP. Our P_i release transients were modeled based on the P_i product that was released from the nucleotide binding site of Eg5. In Figure 9A, acid-quench and P_i release transients at 50 μM MgATP were simulated based on our proposed kinetic mechanism (Scheme 1; Figure 11). In Figure 9B−D, the apoEg5 site concentration was held constant based on the total apoEg5 protein used in the reaction, and the rate constants for all steps in the mechanism were held constant during the simulation, except for the rates of tight ATP binding ($k_{+1'}$), ATP resynthesis (k_{-2}), and P_i release (k_{+3}) as indicated.

RESULTS

ApoEg5 Was Active and Nucleotide-Free. We initiated this study by modifying the purification strategy of Eg5-367 in order to isolate Eg5 in a stable, nucleotide-free state (apoEg5). Our previous Eg5-367 purification strategy yielded a population of motors that retained MgADP bound at the active site (*13*, *22*). The modifications (see *Materials and Methods* for details) were sufficient to isolate apoEg5 at

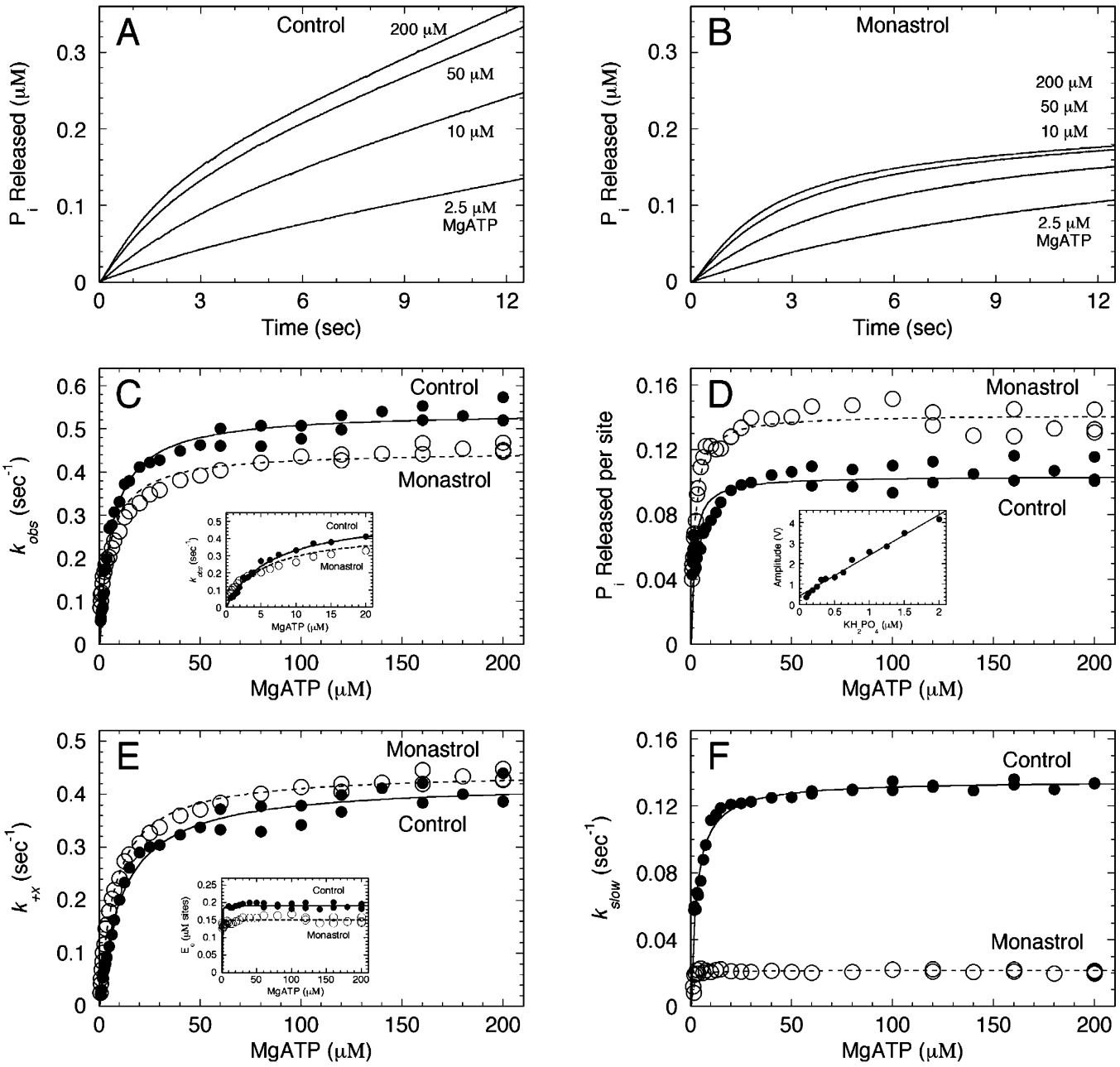

FIGURE 7: Presteady-state kinetics of P_i product release ± monastrol. ApoEg5 plus MDCC-PBP was rapidly mixed with increasing MgATP concentrations, and the fluorescence enhancement of MDCC-PBP binding inorganic phosphate (P_i) was monitored in a stopped-flow instrument. Final concentrations: 1 μM apoEg5, 0 or 150 μM monastrol, 5 μM MDCC-PBP, 0.05 unit/mL PNPase, 75 μM MEG, 0.625−200 μM MgATP. The concentration of P_i product released from apoEg5 (MgATP concentrations are indicated) in the absence (A) and presence (B) of monastrol was plotted as a function of time. Each transient displayed burst kinetics and was fit to eq 6. (C) The exponential rate of phosphate release was plotted versus MgATP concentration. The data were fit to a hyperbola. Control: $k_{max} = 0.54 \pm 0.01$ s^{-1} and $K_{d,ATP} = 6.3 \pm 0.3$ μM. Monastrol: $k_{b,max} = 0.45 \pm 0.01$ s^{-1} and $K_{d,ATP} = 5.1 \pm 0.4$ μM. The inset shows the data from 0 to 20 μM MgATP. (D) The amplitude of the fast exponential phase of each transient was plotted as a function of MgATP concentration. Each data set was fit to a hyperbola. Control: $A_{0,max} = 0.10 \pm 0.003$ P_i/site (19% of expected amplitude based on Eg5 site concentration) and $K_{d,ATP} = 1.6 \pm 0.3$ μM. Monastrol: $A_{0,max} = 0.14 \pm 0.002$ μM (15% of expected amplitude) and $K_{d,ATP} = 1.8 \pm 0.1$ μM. The inset shows the calibration curve used to convert monitored fluorescence voltage to known phosphate concentration. (E) The rate of P_i product release (k_{+3}) determined by fitting the P_i release data to eqs 6−9 was plotted as a function of MgATP concentration, and each data set was fit to a hyperbola. Control: $k_{+1'} = 0.42 \pm 0.006$ s^{-1} and $K_{d,ATP} = 11.5 \pm 0.8$ μM. Monastrol: $k_{+1'} = 0.44 \pm 0.003$ s^{-1} and $K_{d,ATP} = 7.6 \pm 0.3$ μM. The inset shows the modeled Eg5 site concentration (E_0) that contributed to the first ATP turnover as a function of MgATP concentration. (F) The slow rate after P_i release (k_{slow}) was plotted as a function of MgATP concentration, and each data set was fit to a hyperbola. Control: $k_{slow} = 0.14 \pm 0.001$ s^{-1} and $K_{d,ATP} = 2.9 \pm 0.2$ μM. Monastrol: $k_{slow} = 0.022 \pm 0.001$ s^{-1} and $K_{d,ATP} = 0.6 \pm 0.2$ μM.

>99% purity. The apoEg5 protein preparations were tested for activity by measuring the steady-state ATPase kinetics as a function of microtubule concentration at saturating MgATP, and as a function of MgATP concentration at saturating microtubule concentration (Table 1). These experiments demonstrated that, under the same experimental conditions as previous studies (*13*), apoEg5 retained 95−99% of its microtubule-activated ATPase activity. In addition, pulse-chase, acid-quench, and P_i release experiments were performed using the purified apoEg5 in the presence

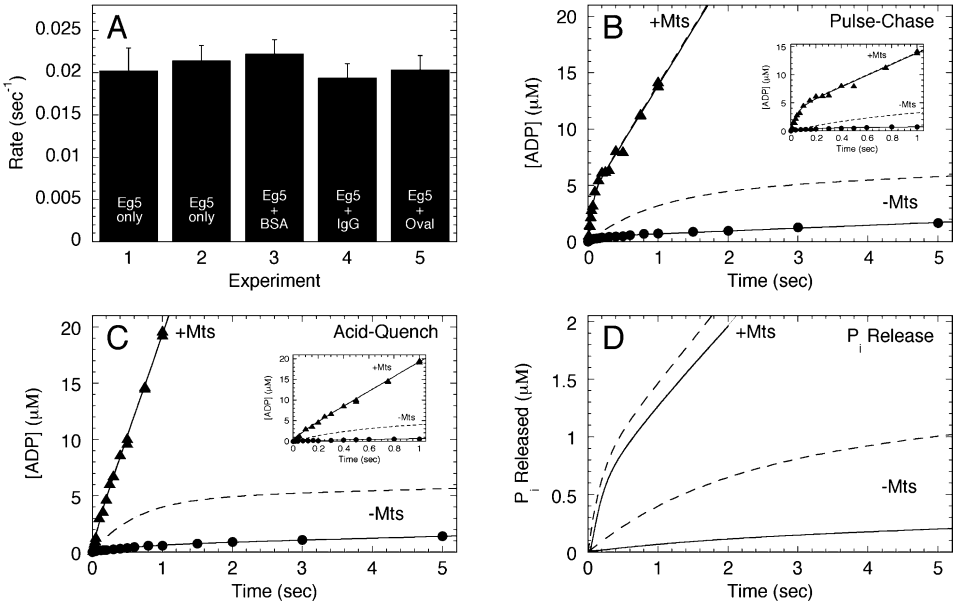

FIGURE 8: Microtubules rescue lowered burst amplitudes. (A) The maximum rate of ATP turnover by apoEg5 was determined under various reaction conditions (as indicated). Final concentrations: 2 μM apoEg5, $\pm$ 0.25 mg/mL BSA, IgG, or ovalbumin, 200 μM [α-^{32}P]-MgATP. Error bars indicate the standard error in the fit of the velocity data for each experiment. (B) Time courses of [α-^{32}P]MgADP product formation for pulse-chase experiments in the absence and presence of microtubules (as indicated). Final concentrations: 5 μM apoEg5, 0 or 6 μM tubulin, 20 μM paclitaxel, 100 μM [α-^{32}P]MgATP, 0 or 100 mM KCl, 10 mM unlabeled MgATP chase. The dashed curves represent expected kinetics of product formation assuming that the entire Eg5 population contributed to the first turnover event. The insets show the data between 0 and 1 s. In the absence of microtubules, the amplitude was 0.09 ADP/site (10% of expected), and in the presence of microtubules, the amplitude was 0.76 ADP/site (98% of expected). (C) Time courses of [α-^{32}P]MgADP product formation for acid-quench experiments in the absence and presence of microtubules (as indicated). Final concentrations: 5 μM apoEg5, 0 or 6 μM tubulin, 20 μM paclitaxel, 100 μM [α-^{32}P]MgATP, 0 or 100 mM KCl. In the absence of microtubules, the amplitude was 0.12 ADP/site (12% of expected), and in the presence of microtubules, the amplitude was 0.26 ADP/site (96% of expected). (D) The concentration of P_i product released from apoEg5 in the absence and presence of microtubules was plotted as a function of time. Final concentrations: 1 μM apoEg5, 0 or 2 μM tubulin, 20 μM paclitaxel, 5 μM MDCC-PBP, 0.05 unit/mL PNPase, 75 μM MEG, 100 μM MgATP, 0 or 100 mM KCl. In the absence of microtubules, the amplitude was 0.11 P_i released/site (14% of expected), and in the presence of microtubules, the amplitude was 0.57 P_i released/site (80% of expected).

of microtubules, and we observed full burst amplitude from each transient, demonstrating that the entire population of apoEg5 sites was fully active.

To determine the nucleotide state of apoEg5, we designed two experiments to directly test the presence of ADP in each apoEg5 preparation. First, we utilized analytical gel filtration to monitor the presence of nucleotide in a sample of apoEg5. We observed a marked decrease in the relative absorbance (A_{259}) at the elution time for ADP when comparing apoEg5 with Eg5·ADP (1:1) or ADP profiles (Figure 1A). After analyzing the ADP peaks (peak apex at 42.7 min) for each condition, apoEg5 appeared to retain approximately 0.07 ADP/Eg5 site compared to Eg5·ADP. However, the sensitivity range of this assay precludes the ability to quantify the precise amount of ADP present in our apoEg5 sample at $\leq$0.07 ADP/site. By simultaneously monitoring intrinsic protein fluorescence (Ex, 280 nm; Em, 340 nm), we did not detect a peak at 16.2 min (void volume), suggesting that there was no detectable aggregation at these conditions (Figure 1A, inset).

Second, we used a MDCC-PBP coupled-assay to detect inorganic phosphate (P_i) product that resulted from the apyrase cleavage reaction. By treating a sample of apoEg5 with apyrase for 60 min, any ADP bound at the active site was released ($>$150 ADP release events at each site) and converted to AMP + P_i (data not shown). When this reaction was mixed with MDCC-PBP, there was very little amplitude associated with the fluorescence enhancement ($<$0.05 P_i/Eg5 site) compared to the Eg5·ADP (1:1) reaction (Figure 1B). This slight increase in fluorescence may be due to contaminating P_i that resides in the apyrase stock solution because of the small amplitude associated with apyrase in the absence of apoEg5 (arrows in Figure 1B). Taken together, these experiments suggest that the apoEg5 preparations were fully active and essentially nucleotide-free.

Steady-State ATPase Reveals Tight ATP Binding, yet Inefficient Catalysis. We characterized apoEg5 by following steady-state ATP turnover as a function of MgATP concentration in the absence of microtubules. Figure 2 shows that the maximum observed rate of MgATP turnover by apoEg5 was 0.02 s^{-1}, similar to former Eg5 preparations (*13*), with a very tight $K_{m,ATP}$ at 0.17 μM. The $K_{m,ATP}$ was greater than 40-fold tighter in the absence of microtubules compared to microtubule-activated steady-state ATPase: 0.17 μM (apoEg5) versus 6.95 μM (Mt·Eg5) (Table 1). However, in the absence of microtubules, the efficiency of apoEg5 ($k_{cat}/K_{m,ATP}$) decreased approximately 5-fold: 0.12 μM^{-1} s^{-1} (apoEg5) versus 0.58 μM^{-1} s^{-1} (Mt·Eg5). These steady-state ATPase kinetics suggest that apoEg5 has a high affinity for substrate, however the slow turnover rate leads to enzymatic inefficiency.

The stability of kinesin family members in the absence of nucleotide has historically been an issue of concern. For *Drosophila* Ncd (Kinesin-14), all attempts to isolate apoNcd under physiological conditions have failed (*14*, *29*), and conventional kinesin (Kinesin-1) in the absence of nucleotide

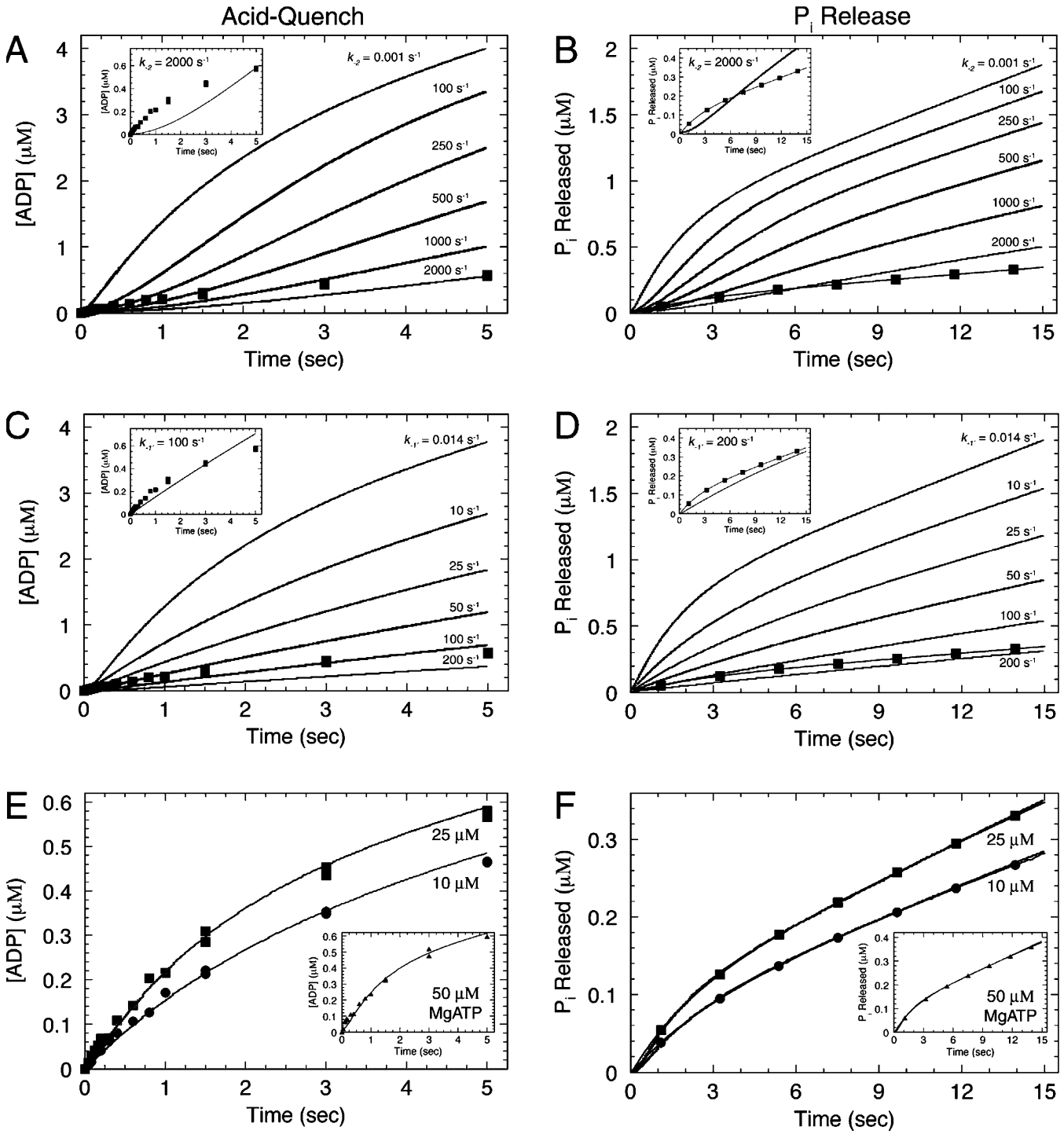

FIGURE 9: ATP hydrolysis reversals and weak ATP binding do not account for reduction in burst amplitude. The acid-quench (A) and P_i release (B) kinetics at 25 μM MgATP were simulated based on a mechanism where the intrinsic rate of ATP resynthesis (k_{-2}) increased from 0.001 s^{-1} to 2000 s^{-1}. Experimental conditions: 4 μM apoEg5 (acid-quench) and 1 μM apoEg5 (P_i release), 25 μM MgATP. Simulated constants: $k_{+1} = 100\ \mu M^{-1}\ s^{-1}$; $k_{-1} = 2700\ s^{-1}$; $k_{+1'} = 1\ s^{-1}$; $k_{-1'} = 0.014\ s^{-1}$; $k_{+2} = 10\ s^{-1}$; $k_{-2} = 0.001$ to $2000\ s^{-1}$ (as indicated); $k_{+3} = 10\ s^{-1}$; $k_{+4} = 0.1\ s^{-1}$; E_0 = total apoEg5 protein. Insets: The "best" fit of the kinetics at 25 μM MgATP where $k_{-2} = 2000\ s^{-1}$. (B) P_i release kinetics simulated to the mechanism used in panel A. (C and D) Simulations of acid-quench and P_i release kinetics, respectively, based on a mechanism where the off-rate for ATP binding increases from 0.014 s^{-1} to 200 s^{-1} (as indicated). Simulated constants: $k_{+1} = 100\ \mu M^{-1}\ s^{-1}$; $k_{-1} = 2700\ s^{-1}$; $k_{+1'} = 1\ s^{-1}$; $k_{-1'} = 0.014-200\ s^{-1}$ (as indicated); $k_{+2} = 10\ s^{-1}$; $k_{-2} = 0.001\ s^{-1}$; $k_{+3} = 10\ s^{-1}$; $k_{+4} = 0.1\ s^{-1}$; E_0 = total apoEg5 protein. Insets: The "best" fit of the kinetics at 25 μM MgATP where $k_{-1'} = 100\ s^{-1}$ (acid-quench) and $200\ s^{-1}$ (P_i release). (E and F) The simulations at 10, 25, and 50 μM MgATP (insets) as proposed for the apoEg5 mechanism from Scheme 1 and Figure 11. Simulated constants: $k_{+1} = 100\ \mu M^{-1}\ s^{-1}$; $k_{-1} = 2700\ s^{-1}$; $k_{+1'} = 1\ s^{-1}$; $k_{-1'} = 0.014\ s^{-1}$; $k_{+2} = 10\ s^{-1}$; $k_{-2} = 0.001\ s^{-1}$; $k_{+3} = 10\ s^{-1}$; $k_{+4} = 0.1\ s^{-1}$; $E_0 = 0.15$. Note: The 50 μM MgATP transients are shown as insets because the data overlay the 25 μM MgATP data, and are difficult to visually resolve when plotted together.

was less stable than Kinesin·ADP, and aggregated at high protein concentrations (*17*). Incubation of apoEg5 at either 4 °C or 22 °C for a time domain that exceeds the duration of any kinetic experiment presented in this manuscript did not significantly affect the ATPase activity (Figure 2, inset). These data suggest that apoEg5 exists as a very stable

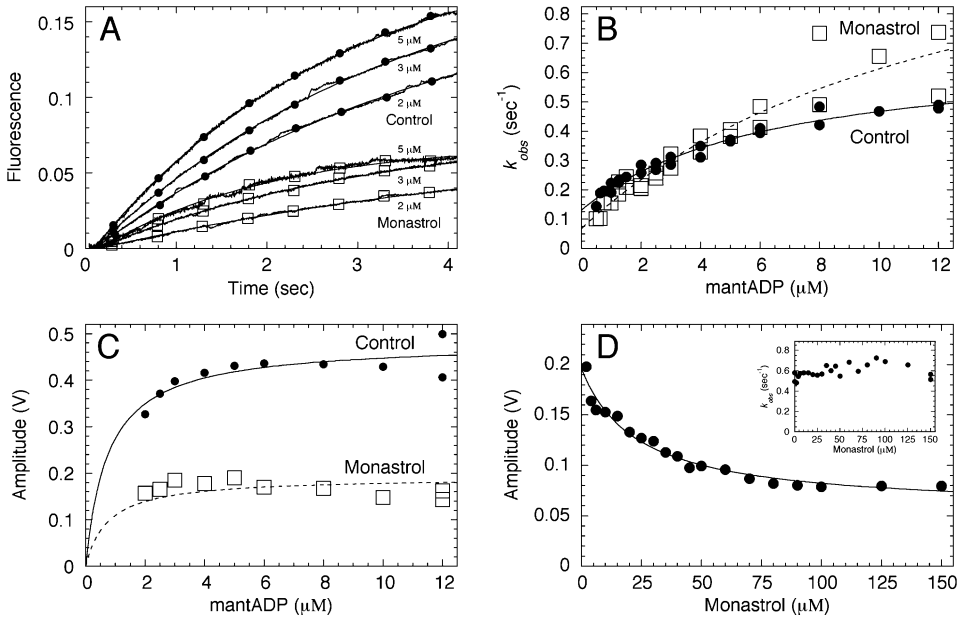

FIGURE 10: MantADP binding to apoEg5 ± monastrol. (A) Representative stopped-flow transients are shown for mantADP binding to apoEg5 in the absence and presence of monastrol. Final concentrations: 0.5 μM apoEg5 for 0.5−2 μM mantADP, 2 μM apoEg5 for 2−12 μM mantADP, 0 or 150 μM monastrol. (B) The observed exponential rate of mantADP binding to apoEg5 was plotted as a function of mantADP concentration. Each data set was fit to eq 5. Control: $k_{-4} = 0.55 \pm 0.04$ s^{-1}, $K_{1/2,mADP} = 6.5 \pm 1.4$ μM, and $k_{+4} = 0.13 \pm 0.01$ s^{-1}. Monastrol: $k_{-4} = 1.3 \pm 0.4$ s^{-1}, $K_{1/2,mADP} = 13.1 \pm 7.7$ μM, and $k_{+4} = 0.07$ s^{-1} ± 0.04. (C) The amplitude of each transient was plotted against mantADP concentration, and each data set was fit to a hyperbola. Maximum amplitude was 0.48 ± 0.02 V for control and 0.19 ± 0.01 V for monastrol. (D) The amplitude of mantADP binding transients plotted as a function of monastrol concentration, and the data were fit to eq 4. Final concentrations: 1 μM apoEg5, 5 μM mantADP, 0−150 μM monastrol. From the fit of the data, $K_{d,S}$ was 23.4 ± 4.8 μM. The inset shows the observed rate of mantADP binding plotted against monastrol concentration.

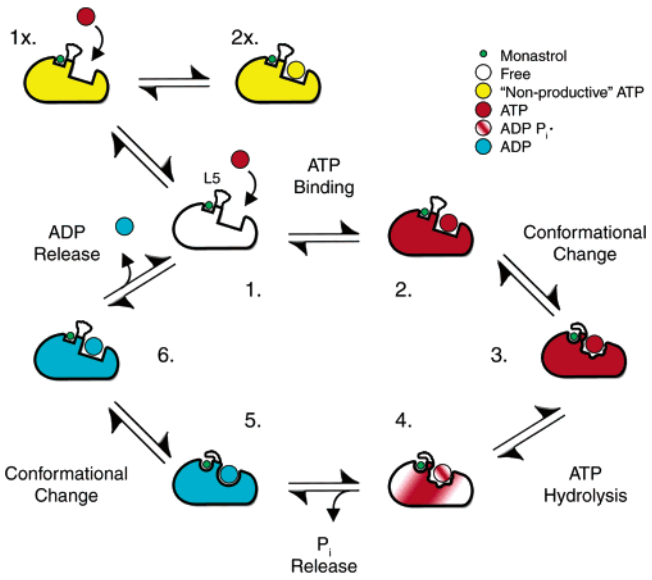

FIGURE 11: Model of apoEg5 ATPase mechanism. The Eg5 motor domain at each stage of the ATPase mechanism is shown with the monastrol binding pocket, the nucleotide binding site, and loop L5 indicated. Species 1, 2, and 6 are shown as binding monastrol weakly, whereas species 3, 4, and 5 are tight-binding states. Species 1x and 2x represent the "nonproductive" apoEg5 state and the "nonproductive" Eg5·ATP collision complex, respectively. The molecules of ATP, ADP, and monastrol are not drawn to scale relative to each other.

monomeric kinesin under these experimental conditions, despite the lack of nucleotide at the active site.

Intrinsic ApoEg5 Fluorescence Enhancement on Nucleotide Binding. The motor domain of human Eg5 contains a single tryptophan residue (W127) that is located on the insertion loop L5 between α2a and α2b [(*30*), see Figure 3E,F]. Loop L5 is eight amino acids longer than the homologous loop in Kinesin-1, exists in a relatively flexible conformation in the Eg5·ADP crystal structure (*30*), and resides in a rigid conformation in the Eg5·ADP·inhibitor crystal structures (*21*, *31*). The primary structure of this loop has been shown to be critical for the binding of and inhibition by specific Eg5 inhibitors (*32*). The conformation of loop L5 in apoEg5 remains unknown. However, when MgATP or MgADP was bound to the nucleotide binding site, a significant enhancement (10.6%) in the steady-state tryptophan fluorescence emission was observed (Figure 3A). To assess the relative accessibility of the tryptophan residue to the solvent, acrylamide quenching studies were performed (Figure 3B). In the absence or presence of nucleotide at the active site, the tryptophan fluorophore was found to have a similar degree of solvent accessibility ($K_{sv} = 4.5$ M^{-1}), suggesting that the residue remains at the surface of the catalytic domain.

To measure the kinetics of the transient increase in tryptophan fluorescence upon nucleotide binding, apoEg5 was rapidly mixed with various nucleotides in a stopped-flow instrument (Figure 3C). MgATP and MgADP appeared to elicit an equivalent fluorescence enhancement at a similar rate and amplitude. The binding of MgAMPPNP, a nonhydrolyzable ATP analogue, also produced a change in tryptophan fluorescence, suggesting that the exponential increase in fluorescence upon MgATP binding corresponds to an event that occurs prior to ATP hydrolysis. Control experiments showed that rapid mixing of apoEg5 with either MgAMP + P_i (1:1) (Figure 3C) or mantAMP + P_i (data not shown) did not elicit a change in fluorescence, providing evidence that apoEg5 does not bind MgAMP + P_i. Taken together, these data argue for a mechanistically relevant

conformational change in loop L5 upon nucleotide binding that results in a change in the environment of the tryptophan residue (Figure 3E,F).

ATP Binding Occurs via a Two-Step Mechanism. The observed rate of MgATP binding by tryptophan fluorescence enhancement was investigated as a function of MgATP concentration. The exponential rate of MgATP binding displayed curvature in the concentration dependence (Figure 3D), indicative of (at least) a two-step mechanism where ATP binding was limited by a first-order isomerization event that follows the formation of a collision complex (Scheme 1) (*33*). The fit of these data provided a maximum rate of MgATP binding ($k_{+1'}$) at 0.54 s^{-1} and the dissociation constant for weak ATP binding ($K_{d,ATP}$) at 2.6 μM. These constants indicate a relatively slow isomerization event that tightens ATP binding to the apoEg5 active site.

The rate of mantATP binding was investigated by direct mant-fluorescence enhancement (Ex, 360 nm; Em, 400-nm cutoff) and by fluorescence resonance energy transfer (FRET) between the tryptophan and the mant-fluorophore (Ex, 295 nm; Em, 400-nm cutoff). Both methods provided similar rates and amplitudes for mantATP binding (data not shown), suggesting that both methods are monitoring the ATP-dependent isomerization step. By monitoring direct mant-fluorescence, we could assess the effect of monastrol on the ATP binding steps in the mechanism. Figure 4C shows that, in the absence or presence of monastrol, there was no significant difference in both the observed rate of mantATP binding (0.85 s^{-1} versus 0.78 s^{-1}) and the $K_{d,mATP}$ (9.9 μM versus 11.4 μM). On the other hand, there was a dramatic decrease in the amplitude of each transient in the presence of monastrol (Figure 4D). We cannot correlate the loss of amplitude to weaker ATP binding due to the similar $K_{d,mATP}$, and the similar ATP binding data obtained from pulse-chase experiments ± monastrol, as discussed below (Figure 5).

A wide variety of chemicals can quench the fluorescence intensity of a fluorophore due to collisional encounters between the two molecules. To test whether monastrol could dynamically quench mant-fluorescence in solution, we analyzed the emission spectrum of mantATP in the absence and presence of monastrol. The emission spectra superimposed (Figure 4E), suggesting that monastrol does not quench mant-fluorescence; therefore, the decreased amplitude in Figure 4D cannot be due to collisional fluorescence quenching by monastrol. Because the collision step for ATP binding comes to equilibrium on a time scale much faster than the rate of the isomerization, this experiment monitors the formation of the tightly bound Eg5*·ATP intermediate. In order for the amplitude to decrease, we assume that monastrol must be bound to the Eg5·ATP collision complex before the first-order isomerization event occurs. One possible explanation for the decreased amplitude is a change in the local environment at the nucleotide binding site when monastrol binds to Eg5, which results in a lower quantum yield from the mant fluorophore when mantAXP binds tightly to the active site. However, the nature of the structural change(s) at the nucleotide binding site upon monastrol binding to the Eg5·ATP collision complex remains speculative, though it does not appear to alter the intrinsic rate constants for the steps of ATP binding.

Pulse-Chase Experiments Reveal Transient Isomerization Intermediate. To measure the presteady-state kinetics of the formation of a tightly bound Eg5*·ATP complex, we performed pulse-chase experiments in a chemical quench-flow instrument. The experimental design assumes that any stably bound substrate will proceed in the forward reaction, while any loosely bound or unbound substrate will be diluted by the excess MgATP present in the chase (*33*). The comparison of the kinetics of product formation obtained by pulse-chase experiments with those obtained by acid-quench experiments can provide (1) direct evidence for the partitioning of the Eg5·ATP intermediate and (2) evidence for a long-lived, stable Eg5*·ATP intermediate prior to ATP hydrolysis. The transients in Figure 5 reveal similar kinetics for ATP binding (pulse-chase) and ATP hydrolysis (acid-quench). However, we did observe a difference in the amplitude of the exponential burst phase for the acid-quench data when the experiment was performed with monastrol (Figures 5 and 6). In the absence of monastrol, the acid-quench $A_{0,max}$ = 0.10 ADP/site and with monastrol, $A_{0,max}$ = 0.15 ADP/site (Figures 5 and 6). The acid-quench data lack a significant initial lag phase preceding the exponential phase, suggesting that the Eg5*·ATP complex proceeds immediately and rapidly toward the chemistry step, and that the observed rate of ATP hydrolysis is limited by the slow conformational change that leads to the tightly bound Eg5*·ATP hydrolysis competent intermediate.

If monastrol were to bind to apoEg5 and stabilize a conformation that results in an obstructed nucleotide binding site where ATP cannot collide, then we would expect an additional reduction in burst amplitude in the presence of monastrol. However, by comparing pulse-chase transients in the absence and presence of monastrol, we found that the amplitudes were similar (A_0 = 0.14 ADP/site). These results suggest that monastrol is not reducing the apoEg5 population that has the potential to bind ATP.

Kinetics of ATP Hydrolysis and P_i Product Release Argue for Rapid Steps in Mechanism. We performed acid-quench experiments as a function of MgATP concentration to determine the maximum observed rate of the ATP hydrolysis step and the apparent $K_{d,ATP}$. Figure 6 shows that, in the absence or presence of monastrol, the maximum observed burst rate of ATP hydrolysis was 1.14 s^{-1} and 0.59 s^{-1}, respectively, while each transient lacked a significant lag phase even at low MgATP concentrations. We also observed a decrease in the expected amplitude for each transient: control = 0.09 ADP/site (13% of expected amplitude) versus monastrol = 0.15 ADP/site (18% of expected amplitude). These kinetics are quite similar to those obtained from our pulse-chase experiments (Figure 5). Based on these data, ATP hydrolysis appears to be limited by the ATP-dependent isomerization event, and after Eg5 binds ATP tightly, it hydrolyzes the nucleotide and presumably releases the P_i product very rapidly.

To directly measure the kinetics of P_i product release from the Eg5 active site after ATP hydrolysis, we performed stopped-flow experiments that detect the change in MDCC-PBP fluorescence upon binding P_i released into solution (*24*). Our P_i release kinetics for apoEg5 suggest a rapid P_i product release step after ATP hydrolysis (Figure 7), thereby rendering the ATP hydrolysis step as kinetically irreversible. We also observed a decrease in burst amplitude (0.10 and 0.14 P_i/site; 19% and 16% of expected amplitude; Figure 7D), which was consistent with our ATP hydrolysis kinetics

(Figure 6). As shown in Figure 7E, the maximum observed rate of P_i product release ($k_{+1'}$) was similar in the absence or presence of monastrol (control, 0.42 s^{-1}; monastrol, 0.44 s^{-1}).

Taken together, these results suggest that after apoEg5 undergoes the ATP-dependent isomerization, it rapidly hydrolyzes ATP and immediately releases P_i product. The rate of ATP hydrolysis by the Mt·Eg5 complex was at least 12-fold faster than the observed rate for apoEg5 (1.14 s^{-1} versus 13.3 s^{-1}) (*13*). A fast reaction that occurs in series with a slow reaction will proceed at the rate of the slow reaction (*33*); thus the rate of ATP hydrolysis will be limited by the relatively slow, ATP-promoted isomerization step. There was not a considerable lag phase in the ATP hydrolysis kinetics, thus implying that the two steps in the mechanism occur at significantly different rates (>10-fold) (*33*). Likewise, the release of P_i product was measured at the same observed rate as the isomerization step without a substantial initial lag phase corresponding to ATP binding and ATP hydrolysis. Taken together, these data indicate that the Eg5*·ATP and the Eg5·ADP·P_i intermediates are kinetically transient. Our pulse-chase data support this hypothesis given the similar rates and amplitudes of the pulse-chase transients compared to acid-quench transients (Figure 5).

Reduction of Product Burst Amplitude Rescued by Microtubules. Data sets from pulse-chase, acid-quench, and P_i product release experiments show a considerable decrease in amplitude of the fast exponential phase for each transient. Several factors could contribute to the reduced amplitude: (1) a slightly heterogeneous apoEg5 preparation where a subpopulation (<5%) retains ADP at the nucleotide binding site, (2) inactive apoEg5, (3) weak ATP binding, (4) reversals at the ATP hydrolysis step, and/or (5) "nonproductive" apoEg5 enzyme that cannot generate the ATP-promoted structural transitions required to proceed forward to ATP hydrolysis. A slight heterogeneity in the apoEg5 population and inactive apoEg5 protein cannot fully explain the reduced burst amplitude based on the results presented in Figure 1. In addition, there is no evidence for weak ATP binding. In fact, the $K_{m,ATP}$ was 0.17 μM. As already mentioned, an increase in the intrinsic rate of ATP resynthesis (k_{-2}) cannot explain the observed kinetics of ATP hydrolysis and P_i product release (Figure 9; see further details below). To evaluate whether adsorption of apoEg5 to the walls of the reaction tubes was leading to a loss in enzymatic sites, we followed steady-state ATP turnover in the presence of BSA, IgG, or ovalbumin at 0.25 mg/mL. We did not observe a significant difference in the rate of ATP turnover by adding the additional protein (Figure 8A). Interestingly, the steady-state ATPase activity of apoEg5 in the presence of microtubules provided a maximum rate of ATP turnover that was suggestive of fully active protein (Table 1).

To directly measure the activity of the apoEg5 protein used in the presteady-state experiments, we repeated the experiments with the Mt·Eg5 complex. When pulse-chase, acid-quench, and P_i product release experiments were performed with the Mt·Eg5 complex, we observed >95% of the expected amplitude for the burst of product formation (Figure 8B-D), suggesting that all apoEg5 protein has the potential for ATP binding and hydrolysis during the first turnover event. These data are consistent with the hypothesis that there is a subpopulation of apoEg5 that cannot drive the structural transitions for ATP hydrolysis; therefore, this population remains silent in the pulse-chase, acid-quench, and phosphate release kinetics in the absence of microtubules leading to the reduction in burst amplitude.

ATP Hydrolysis Reversals and Weak ATP Binding Do Not Explain the Reduction in Burst Amplitude. Two possible explanations for the reduction in burst amplitude are an internal equilibrium that is established at the ATP hydrolysis step, where ATP hydrolysis is followed by ATP resynthesis, and weak ATP binding. Experiments to directly test the first hypothesis (intermediate O^{18} exchange) have not been employed in this study. However, we used DynaFit software to simulate the kinetics of product formation when the intrinsic rate constant for ATP resynthesis (k_{-2}) increases, while the total apoEg5 site concentration remained constant based on the conditions of the experiment. As we increased the value for k_{-2}, the burst amplitude was reduced; however, the initial lag phase was substantially increased, and the simulated curves did not follow the actual experimental data at any value of k_{-2} tested (Figure 9A,B). We also tried increasing the off-rate of ATP binding ($k_{-1'}$) during these simulations, but again were unable to attain a good fit of the data (Figure 9C,D). We were unable to find a combination of rate constants for the entire apoEg5 population reporting for ATP binding, ATP hydrolysis, P_i release, and ADP release (Scheme 1) that provided a reasonable fit of the data.

On the other hand, if we decreased the apoEg5 concentration to a value similar to the fraction of sites that reported during ATP hydrolysis and P_i release experiments (~15%), the maximum rate of ATP binding at 1 s^{-1}, the forward rates of ATP hydrolysis and P_i release at 10 s^{-1}, and the rate of ADP release at 0.1 s^{-1}, we were able to simulate transients at 10, 25, and 50 μM MgATP within the error of the experiment (Figure 9E,F). For the 25 μM MgATP transient, the mean square of the least-squares fit using DynaFit was 0.00023 and 0.0000033 for the acid-quench and the P_i release transients, respectively (Figure 9E,F), whereas, by adjusting the rate constants and holding the apoEg5 concentration fixed (as described above), the "best" least-squares fit provided a mean square of 0.013 and 0.0031 for the acid-quench and P_i release transients, respectively (Figure 9A−D, insets). These simulation results suggest that our proposed mechanism, in which a substantial fraction of "nonproductive" apoEg5 is unable to properly bind and hydrolyze ATP, remains the best explanation for the observed kinetics in the presteady-state experiments.

MantADP Binding Occurs via Two-Step Process. We performed mantADP binding experiments in the absence and presence of monastrol to determine the kinetics of ADP binding and release from apoEg5 (Figure 10, Scheme 2). We observed hyperbolic mantADP binding kinetics, which is indicative of at least two-step binding of ADP as observed for ATP (Figures 3 and 4). The off-rate for mantADP binding, as determined from the extrapolation of the fit of the data back to the *y*-axis (control, 0.13 s^{-1}; monastrol, 0.08 s^{-1}), was similar to the rate of the slow step after P_i product release that limits steady-state ATP turnover (control, 0.14 s^{-1}; monastrol, 0.022 s^{-1}) (Figure 7F). The results in Figure 10 document two ADP intermediates (Scheme 2): the Eg5·ADP collision complex and the Eg5*·ADP intermediate

detected by saturation of the observed rate for mantADP binding.

In the presence of monastrol, we observed a faster rate for the isomerization of the Eg5·mantADP collision complex (control 0.55 s^{-1} versus monastrol 1.3 s^{-1}) (Figure 10B). In addition, the amplitude of each transient was decreased to a similar extent as the mantATP binding transients (compare Figure 4D with Figure 10C), suggesting that an alteration of the nucleotide binding site environment by monastrol lowers the quantum yield of mantADP as well.

Monastrol Slows ADP Product Release. As published previously (*22*), [α-^{32}P]ADP release from Eg5 was a slow step in the absence of monastrol and was slowed further in the presence of monastrol (0.05 s^{-1} versus 0.007 s^{-1}). This is consistent with the observation of presteady-state burst kinetics in the pulse-chase, acid-quench, and P_i release experiments presented in this manuscript. The data for acid-quench and P_i release experiments were modeled to a two-step irreversible mechanism to obtain the rate constants of ATP hydrolysis (k_{+2}) and P_i product release (k_{+3}), respectively, and the rate constant for the slow step after P_i release (ADP release) that limits steady-state ATP turnover (k_{slow}). For these experiments, k_{slow} was 0.14 s^{-1} in the absence of monastrol and 0.025 s^{-1} in the presence of monastrol, and the maximum observed rate of ATP turnover was inhibited by monastrol (0.019 s^{-1} to 0.003 s^{-1}). The inhibition of the rate of ADP release correlates well with the reduction in the rate of ATP turnover; however, there is a 7-fold difference between the rate of ADP release and the steady-state k_{cat} under both conditions. Our hypothesis for this difference is a subpopulation of apoEg5 that either cannot bind ATP or cannot promote the conformational change to generate the ATP hydrolysis-competent intermediate. Nevertheless, this "nonproductive" subpopulation of apoEg5 is present in the absence of monastrol, suggesting that it is not the result of monastrol binding.

Monastrol Binds Weakly to the Eg5·AXP Collision Complexes. In both mantATP and mantADP binding experiments, we observed a marked decrease in the amplitude of each transient in the presence of monastrol. To determine the monastrol concentration-dependence of this phenomenon, we performed mantAXP binding experiments as a function of monastrol concentration (Figure 4F and Figure 10D). In both experiments, we obtained an apparent $K_{d,S} = 25\ \mu M$, which was an order of magnitude weaker than the apparent $K_{d,S}$ measured by steady-state ATPase inhibition: $K_{d,S} = 2.3\ \mu M$ (see Figure 1A in ref *22*). In addition, the results in Figure 3C show that MgADP and MgATP trigger the enhancement of tryptophan fluorescence at the same rate and amplitude, suggesting that this change in fluorescence is a readout of the same structural transition of loop L5 achieved by either ADP or ATP binding. There is not a detectable signal for direct binding of monastrol to apoEg5, yet these results indicate that monastrol binds by a two-step mechanism (Figure 11). In the first step, monastrol collides and binds weakly to apoEg5 in the absence of nucleotide, and its affinity for Eg5 is tightened by the ATP-dependent (or ADP-dependent) isomerization. We propose that this nucleotide-dependent isomerization is correlated with the "closing" of loop L5, which promotes both tight nucleotide and tight monastrol binding and was detected experimentally by the enhancement of the tryptophan fluorescence (Figure 3). The results suggest that the monastrol weak binding state is detected by the $K_{d,S}$ at 25 μM and that the isomerization to the second intermediate is detected by the $K_{d,S}$ at 2.3 μM. This closed state achieved by tight nucleotide and monastrol binding would slow the rate of ADP release from the active site. We propose for ADP release that loop L5 adopts the "open" conformation, thus the affinity for ADP is weakened (Figure 11).

DISCUSSION

In this study, we have combined steady-state and presteady-state methodologies to define a minimal mechanism of the mitotic Eg5 ATPase in the absence of microtubules (Figure 11, Table 1). By comparing the basal Eg5 ATPase to the microtubule-activated ATPase (*13*), we were able to gain insight into the amplification and acceleration of the structural transitions that dictate the microtubule-dependent activation. In addition, we have investigated the mechanistic basis for the allosteric inhibition of the basal Eg5 ATPase by monastrol.

ApoEg5 Was Active, Stable, and Nucleotide-Free. A critical factor for this study was the characterization of the apoEg5 protein obtained from our adopted purification strategy. Steady-state ATPase assays were performed in the absence and presence of microtubules, and the activity under the same experimental conditions was found to be comparable to former Eg5 preparations [Table 1 (*13*, *22*)]. Remarkably, the apoEg5 protein was very stable (Figure 2, inset), despite the lack of ADP at the active site (Figure 1). Therefore, our apoEg5 site concentration can be reasonably estimated to >95% of total protein concentration determined by Bradford assays.

"Nonproductive" versus "Productive" ApoEg5 States Are in Rapid Equilibrium. We observed a dramatic difference between the steady-state k_{cat} and the rate of ADP release (rate-limiting step). We also observed a reduction in the expected amplitude for our pulse-chase, acid-quench, and P_i product release experiments. When we divide the maximum velocity of steady-state ATP turnover (0.0017 μM ADP·s^{-1}) by the concentration of apoEg5 sites reported during the presteady-state experiments (0.013−0.019 μM), we obtain a steady-state k_{cat} at 0.09−0.13 s^{-1}, which is consistent with the rate of ADP release. Control experiments in the presence of microtubules demonstrated that >95% of the Eg5 population can contribute to the first ATP turnover event (Figure 8). These data seem to suggest that, in the absence of microtubules, there is a subpopulation of apoEg5 that is unable to drive the ATP-dependent structural transitions that are required for ATP hydrolysis during both the first turnover and subsequent ATP turnover events (Figure 11). In contrast, when apoEg5 was bound to microtubules, we observed the entire Eg5 population in the "productive" state, and thus able to properly bind and hydrolyze ATP (Figure 8). These results provide evidence for the role of microtubules in amplifying and accelerating the structural transitions that account for Eg5's ATPase efficiency.

Substrate Binding Was Dramatically Slower. The kinetics of ATP binding were determined by measuring the intrinsic tryptophan fluorescence enhancement upon MgATP binding (Figure 3), as well as monitoring the fluorescence change upon mantATP binding at the apoEg5 active site (Figure 4).

Both experiments demonstrated that substrate binding to apoEg5 seemed to occur in at least two distinct kinetic steps: formation of the initial weak-binding collision complex (Eg5·ATP) followed by an isomerization of the collision complex that leads to tightened ATP binding (Eg5*·ATP). In comparison to the substrate binding kinetics for the Mt·Eg5 complex, we found that Eg5 has a similar affinity for ATP: $K_{d,mATP} = 9.9\ \mu M$ (apoEg5) versus 7.9 μM (Mt·Eg5) (*22*). However, the rate of the isomerization step was approximately 55-fold slower for apoEg5: 0.85 s^{-1} (apoEg5) versus 47.0 s^{-1} (Mt·Eg5) (*22*). We propose that the microtubule amplifies and accelerates the structural transitions in the Eg5 motor domain that lead to tight ATP binding. A recent study suggests that a conformational change in the nucleotide binding site via the switch-1 region occurs when kinesin-family motors bind to microtubules (*34*). The microtubule seems to lower the energy barrier for conformational changes in Eg5's switch regions, thus rendering the kinetic steps of ATP binding much faster.

Movement of Loop L5 Correlates with Movement of the Switch Regions. The insertion loop L5 that interrupts helix α2 varies considerably in sequence among different subfamilies of kinesins and, for Eg5, seems to be a "hotspot" for specific inhibitors (*21*, *31*, *32*). Certainly this loop was not designed to facilitate the binding of these inhibitors, but likely undergoes structural transitions during the ATPase cycle that correlates with the movements of the functional components of the Eg5 catalytic domain, such as switch-1 and switch-2 regions. Loop L5 is located in close proximity to the N-terminal end of helix α3, which in turn is connected to loop L9 that contains the γ-phosphate sensing residue (S233) (Figure 3E,F). Loop L5 contains the lone tryptophan residue in the human Eg5 motor domain. In this study, we have demonstrated a nucleotide-dependent enhancement of tryptophan fluorescence, which marks the conformational changes that occur upon tight ATP or ADP binding to the Eg5 active site. This conformation change in loop L5 appears to occur before ATP hydrolysis, due to the fluorescence enhancement upon AMPPNP binding, and also seems to persist after ATP hydrolysis and P_i product release, due to the sustained fluorescence intensity over the time course for the first turnover event. Thus, we hypothesize that the movement of loop L5 is tightly correlated to Eg5's mechanochemical cycle. A recent study demonstrated that if loop L5 from Eg5 were replaced with a homologous loop from Kinesin-1, the ATPase in the absence of microtubules decreased ~2-fold, thus supporting our hypothesis (*32*).

All Eg5 crystal structures solved to date contain ADP at the active site (*21*, *31*, *32*). Interestingly, the Eg5·ADP·inhibitor crystal structures display an altered conformation of loop L5 compared to the Eg5·ADP structure. The interpretation of this structure was a conformational change in loop L5 that was "induced" by the inhibitor binding. However, our data argue that this "open" to "closed" conformational change in loop L5 occurs normally during the Eg5 ATPase mechanochemical cycle. In addition, when the inhibitor is present in its allosteric site, it stabilizes this $Eg5_S$·ADP conformation of loop L5, and thus slows ADP product release dramatically. Our mantADP binding data suggest that ADP binds to apoEg5 in a two-step fashion, with a rapid-equilibrium collision step followed by an isomerization of the Eg5·ADP collision complex to tighten the binding of ADP. We also observed an enhancement of tryptophan fluorescence upon ADP binding that was quite similar in rate and amplitude when compared with ATP binding. Therefore, we propose that the structural transition coupled to ADP product release is rate-limiting in the apoEg5 mechanism, and the conformation of loop L5 correlates with this structural transition to the "open" state (Figure 11; Species 6).

Monastrol Binding Occurs via a Two-Step Mechanism. As previously reported, the ATP binding steps of the Mt·Eg5 ATPase mechanism were not affected by monastrol (*22*). As demonstrated in this study, monastrol also does not significantly affect the kinetics of ATP binding, ATP hydrolysis, and P_i release in the absence of microtubules. However, monastrol does appear to bind the Eg5·ATP and Eg5·ADP collision complexes, and surprisingly alters the nucleotide binding site environment in a manner that leads to a reduction in the quantum yield from mantAXP fluorescence. Monastrol does not quench the fluorescence of the mant-fluorophore in solution, and ATP binding does not seem to be weakened in the presence of monastrol. A slight decrease in amplitude was also observed in similar experiments performed with the Mt·Eg5 complex (*22*), which suggests that a similar nucleotide binding site environment may be attained when monastrol binds the Mt·Eg5·ATP collision complex.

In this study, we found that monastrol binds to the Eg5·ATP or Eg5·ADP collision complex more weakly than detected by steady-state turnover [25 μM versus 2.3 μM (*22*)]. We propose that monastrol binds weakly to the nucleotide-free state and Eg5·AXP collision complexes due to the "open" conformation of loop L5, and concomitantly with tight nucleotide binding, a conformational change in loop L5 occurs to "close" the inhibitor pocket, thus dramatically increasing Eg5's affinity for monastrol. A communication pathway from the nucleotide binding site to loop L5 is possibly mediated through a conformational change in the switch-1 region and is relayed through helix α3 to the insertion loop L5, which is located in close proximity to the N-terminal end of helix α3 (Figure 3E).

In summary, the minimal apoEg5 ATPase mechanism shares similarities in the kinetic steps required for ATP turnover compared to the Mt·Eg5 mechanism; however, the rate constants that define these steps show dramatic differences. ATP binding occurs via a two-step process for both pathways, yet the isomerization of the Eg5·ATP collision complex is dramatically slower for apoEg5. The microtubule appears to amplify and accelerate the conformational changes that tighten ATP binding. ATP hydrolysis and P_i product release are rapid steps in the mechanism, yet the observed rate constants are significantly slower in the absence of microtubules. In addition, there is no kinetic evidence for ATP hydrolysis reversals for apoEg5 as observed for myosin (*35*). The structural transition(s) of the Eg5·ADP intermediate coupled to ADP release is the rate-limiting step in the pathway, and this step is dramatically accelerated upon binding to the microtubule (0.05 s^{-1} to 35 s^{-1}) such that ADP release no longer limits steady-state ATP turnover for the Mt·Eg5 complex. Monastrol appears to bind weakly to apoEg5, but after ATP binding and the ATP-dependent isomerization, apoEg5 binds monastrol tightly. This monastrol-stabilized state inhibits the conformational change needed

for rapid ADP product release. Therefore, monastrol has stabilized a mechanistically relevant structural state of the Eg5 to elicit its inhibitory effect upon the ATPase cycle.

ACKNOWLEDGMENT

We thank Dr. Wasyl Halczenko and Dr. George Hartman (Merck Research Laboratories, West Point, PA) for the gift of *S*-monastrol, Hans Wildschutte and Dr. Jeffery Lawrence (University of Pittsburgh) for their assistance with the fluorimeter, and our colleagues, Troy C. Krzysiak and Lisa R. Sproul, for their intellectual discussions and helpful comments during this study. We are also grateful to Dr. F. Jon Kull (Dartmouth College) for his insightful comments on this manuscript.

REFERENCES

1. Vale, R. D., and Milligan, R. A. (2000) The way things move: looking under the hood of molecular motor proteins, *Science 288*, 88−95.
2. Holmes, K. C., and Geeves, M. A. (2000) The structural basis of muscle contraction, *Philos. Trans. R. Soc. London, Ser. B 355*, 419−31.
3. Kikkawa, M., Sablin, E. P., Okada, Y., Yajima, H., Fletterick, R. J., and Hirokawa, N. (2001) Switch-based mechanism of kinesin motors, *Nature 411*, 439−45.
4. Kull, F. J., and Endow, S. A. (2002) Kinesin: switch I & II and the motor mechanism, *J. Cell Sci. 115*, 15−23.
5. Vale, R. D. (2003) The molecular motor toolbox for intracellular transport, *Cell 112*, 467−80.
6. Endow, S. A. (2003) Kinesin motors as molecular machines, *Bioessays 25*, 1212−9.
7. Schliwa, M., and Woehlke, G. (2003) Molecular motors, *Nature 422*, 759−65.
8. Cooke, R. (2004) The sliding filament model: 1972-2004, *J. Gen. Physiol. 123*, 643−56.
9. Hackney, D. D. (1996) The kinetic cycles of myosin, kinesin, and dynein, *Annu. Rev. Physiol. 58*, 731−50.
10. Moyer, M. L., Gilbert, S. P., and Johnson, K. A. (1996) Purification and characterization of two monomeric kinesin constructs, *Biochemistry 35*, 6321−9.
11. Ma, Y. Z., and Taylor, E. W. (1997) Kinetic mechanism of a monomeric kinesin construct, *J. Biol. Chem. 272*, 717−23.
12. Moyer, M. L., Gilbert, S. P., and Johnson, K. A. (1998) Pathway of ATP hydrolysis by monomeric and dimeric kinesin, *Biochemistry 37*, 800−13.
13. Cochran, J. C., Sontag, C. A., Maliga, Z., Kapoor, T. M., Correia, J. J., and Gilbert, S. P. (2004) Mechanistic analysis of the mitotic Kinesin Eg5, *J. Biol. Chem. 279*, 38861−70.
14. Pechatnikova, E., and Taylor, E. W. (1997) Kinetic mechanism of monomeric non-claret disjunctional protein (Ncd) ATPase, *J. Biol. Chem. 272*, 30735−40.
15. Mackey, A. T., and Gilbert, S. P. (2000) Moving a microtubule may require two heads: a kinetic investigation of monomeric Ncd, *Biochemistry 39*, 1346−55.
16. Mackey, A. T., and Gilbert, S. P. (2003) The ATPase cross-bridge cycle of the Kar3 motor domain. Implications for single head motility, *J. Biol. Chem. 278*, 3527−35.
17. Sadhu, A., and Taylor, E. W. (1992) A kinetic study of the kinesin ATPase, *J. Biol. Chem. 267*, 11352−9.
18. Muller, J., Marx, A., Sack, S., Song, Y. H., and Mandelkow, E. (1999) The structure of the nucleotide-binding site of kinesin, *Biol. Chem. 380*, 981−92.
19. Maliga, Z., Kapoor, T. M., and Mitchison, T. J. (2002) Evidence that monastrol is an allosteric inhibitor of the mitotic kinesin Eg5, *Chem. Biol. 9*, 989−96.
20. DeBonis, S., Simorre, J. P., Crevel, I., Lebeau, L., Skoufias, D. A., Blangy, A., Ebel, C., Gans, P., Cross, R., Hackney, D. D., Wade, R. H., and Kozielski, F. (2003) Interaction of the mitotic inhibitor monastrol with human kinesin Eg5, *Biochemistry 42*, 338−49.
21. Yan, Y., Sardana, V., Xu, B., Homnick, C., Halczenko, W., Buser, C. A., Schaber, M., Hartman, G. D., Huber, H. E., and Kuo, L. C. (2004) Inhibition of a mitotic motor protein: where, how, and conformational consequences, *J. Mol. Biol. 335*, 547−54.
22. Cochran, J. C., Gatial, J. E., 3rd, Kapoor, T. M., and Gilbert, S. P. (2005) Monastrol inhibition of the mitotic kinesin Eg5, *J. Biol. Chem. 280*, 12658−67.
23. Hackney, D. D., Malik, A. S., and Wright, K. W. (1989) Nucleotide-free kinesin hydrolyzes ATP with burst kinetics, *J. Biol. Chem. 264*, 15943−8.
24. Brune, M., Hunter, J. L., Corrie, J. E., and Webb, M. R. (1994) Direct, real-time measurement of rapid inorganic phosphate release using a novel fluorescent probe and its application to actomyosin subfragment 1 ATPase, *Biochemistry 33*, 8262−71.
25. Gilbert, S. P., Webb, M. R., Brune, M., and Johnson, K. A. (1995) Pathway of processive ATP hydrolysis by kinesin, *Nature 373*, 671−6.
26. Gilbert, S. P., and Mackey, A. T. (2000) Kinetics: a tool to study molecular motors, *Methods 22*, 337−54.
27. Klumpp, L. M., Hoenger, A., and Gilbert, S. P. (2004) Kinesin's second step, *Proc. Natl. Acad. Sci. U.S.A. 101*, 3444−9.
28. Kuzmic, P. (1996) Program DYNAFIT for the analysis of enzyme kinetic data: application to HIV proteinase, *Anal. Biochem. 237*, 260−73.
29. Morii, H., Shimizu, T., Mizuno, N., Edamatsu, M., Ogawa, K., Shimizu, Y., and Toyoshima, Y. Y. (2005) Removal of tightly bound ADP induces distinct structural changes of the two tryptophan-containing regions of the ncd motor domain, *J. Biochem. (Tokyo) 138*, 95−104.
30. Turner, J., Anderson, R., Guo, J., Beraud, C., Fletterick, R., and Sakowicz, R. (2001) Crystal structure of the mitotic spindle kinesin Eg5 reveals a novel conformation of the neck-linker, *J. Biol. Chem. 276*, 25496−502.
31. Cox, C. D., Breslin, M. J., Mariano, B. J., Coleman, P. J., Buser, C. A., Walsh, E. S., Hamilton, K., Huber, H. E., Kohl, N. E., Torrent, M., Yan, Y., Kuo, L. C., and Hartman, G. D. (2005) Kinesin spindle protein (KSP) inhibitors. Part 1: The discovery of 3,5-diaryl-4,5-dihydropyrazoles as potent and selective inhibitors of the mitotic kinesin KSP, *Bioorg. Med. Chem. Lett. 15*, 2041−5.
32. Brier, S., Lemaire, D., DeBonis, S., Forest, E., and Kozielski, F. (2004) Identification of the Protein Binding Region of *S*-Trityl-L-cysteine, a New Potent Inhibitor of the Mitotic Kinesin Eg5, *Biochemistry 43*, 13072−82.
33. Johnson, K. A. (1992) Transient-state kinetic analysis of enzyme reaction pathways, in *The Enzymes*, pp 1−61, Academic Press, New York.
34. Naber, N., Rice, S., Matuska, M., Vale, R. D., Cooke, R., and Pate, E. (2003) EPR Spectroscopy Shows a Microtubule-Dependent Conformational Change in the Kinesin Switch 1 Domain, *Biophys. J. 84*, 3190−6.
35. Bagshaw, C. R., Trentham, D. R., Wolcott, R. G., and Boyer, P. D. (1975) Oxygen exchange in the gamma-phosphoryl group of protein-bound ATP during Mg2+-dependent adenosine triphosphatase activity of myosin, *Proc. Natl. Acad. Sci. U.S.A. 72*, 2592−6.

BI051724W